Silica-rich Melts in Quartz Xenoliths from Vulcano Island and their Bearing on Processes of Crustal Anatexis and Crust–Magma Interaction beneath the Aeolian Arc, Southern Italy

MARIA-LUCE FREZZOTTI[1]*, ANGELO PECCERILLO[2], VITTORIO ZANON[2] AND IGOR NIKOGOSIAN[3]

[1]DIPARTIMENTO DI SCIENZE DELLA TERRA, UNIVERSITÀ DEGLI STUDI DI SIENA, VIA LATERINA 8, I-53100 SIENA, ITALY

[2]DIPARTIMENTO DI SCIENZE DELLA TERRA, UNIVERSITÀ DEGLI STUDI DI PERUGIA, P.ZZA UNIVERSITÀ 1, I-06100 PERUGIA, ITALY

[3]FACULTEIT VOOR AARD- EN LEVENS-WETENSCHAPPEN, VRIJE UNIVERSITEIT, DE BOELELAAN 1085, 1081-HV AMSTERDAM, THE NETHERLANDS

Quartz-rich xenoliths in lavas and pyroclastic rocks from Vulcano Island, part of the Aeolian arc, Italy, contain silicic melt inclusions with high SiO_2 (73–80 wt %) and K_2O (3–6 wt %) contents. Two types of inclusions can be distinguished based on their time of entrapment and incompatible trace element (ITE) concentrations. One type (late, ITE-enriched inclusions) has trace element characteristics that resemble those of the metamorphic rocks of the Calabro-Peloritano basement of the adjacent mainland. Other inclusions (early, ITE-depleted) have variable Ba, Rb, Sr and Cs, and low Nb, Zr and rare earth element (REE) contents. Their REE patterns are unfractionated, with a marked positive Eu anomaly. Geochemical modelling suggests that the ITE-depleted inclusions cannot be derived from equilibrium melting of Calabro-Peloritano metamorphic rocks. ITE-enriched inclusions can be modelled by large degrees (>80%) of melting of basement gneisses and schists, leaving a quartz-rich residue represented by the quartz-rich xenoliths. Glass inclusions in quartz-rich xenoliths represent potential contaminants of Aeolian arc magmas. Interaction between calc-alkaline magmas and crustal anatectic melts with a composition similar to the analysed inclusions may generate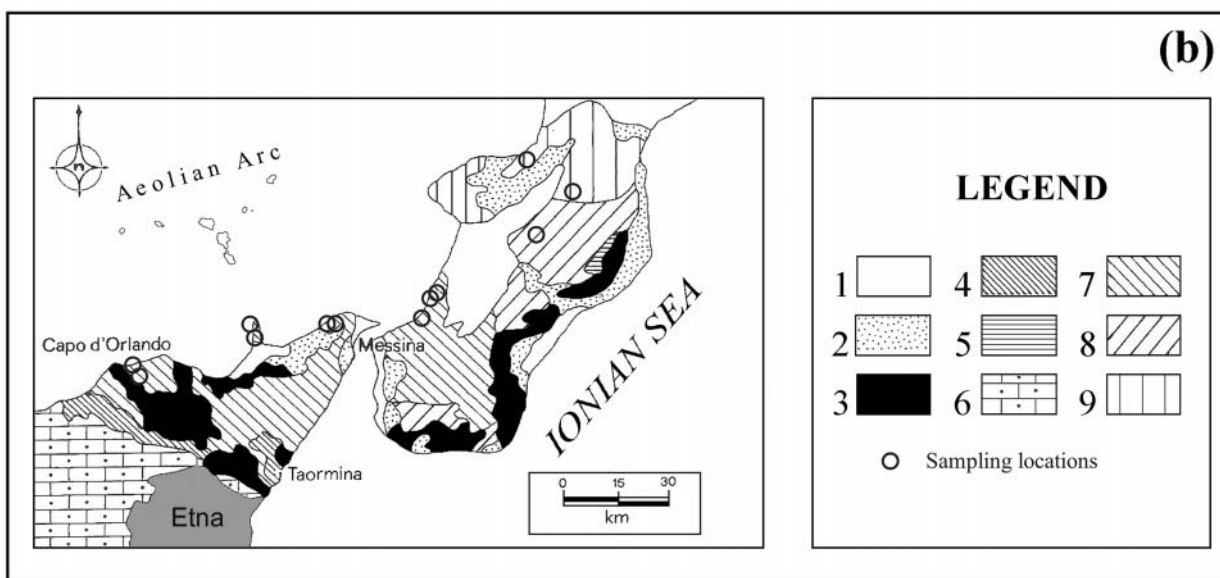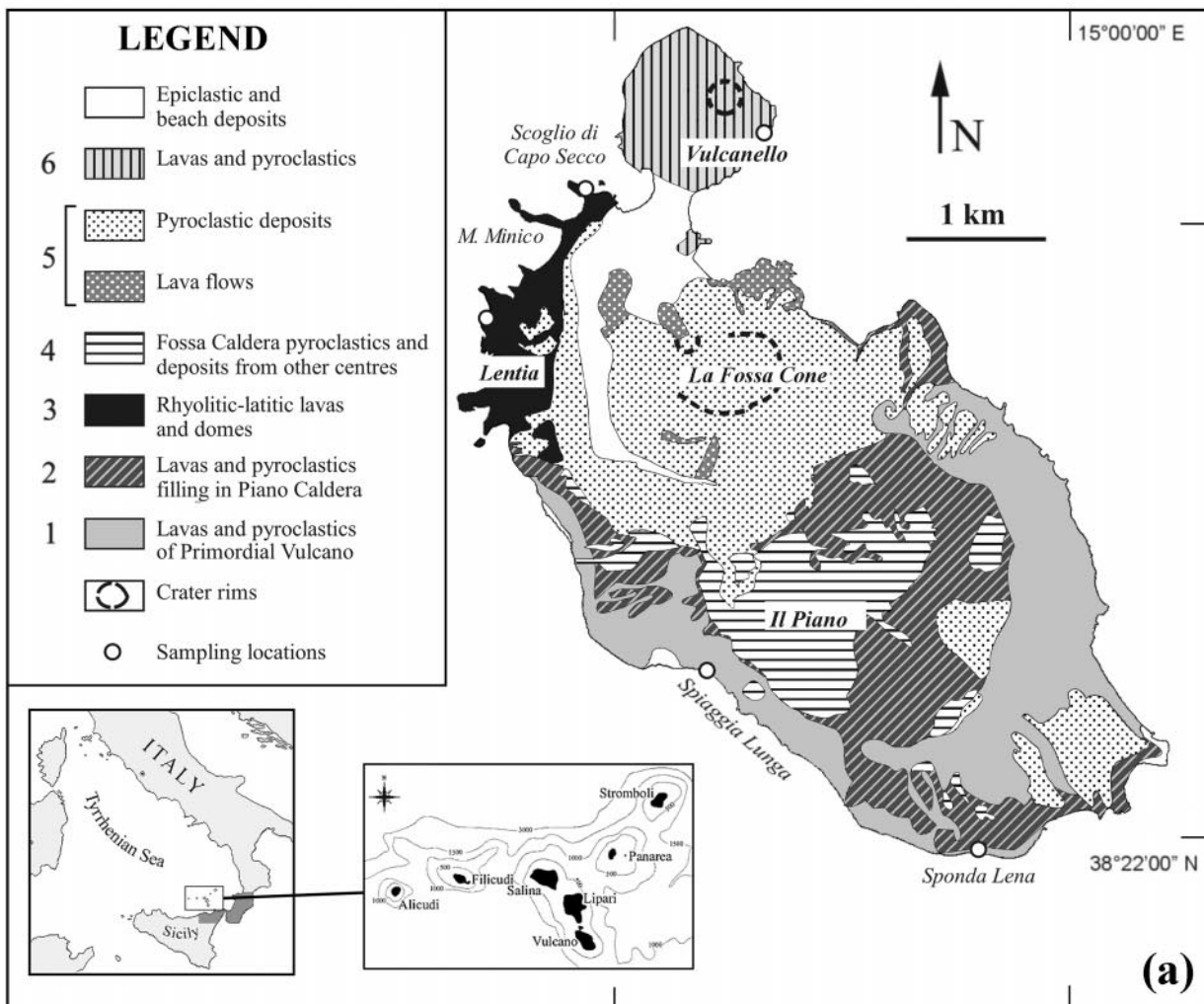 significant enrichment in potassium in the magmas. However, ITE contents of the melt inclusions are comparable with or lower than those of Vulcano calc-alkaline and potassic rocks. This precludes the possibility that potassic magmas in the Aeolian arc may originate from calc-alkaline parents through different degrees of incorporation of crustal melts.

KEY WORDS: *melt inclusions; crustal anatexis; magma assimilation; xenoliths; Vulcano Island*

INTRODUCTION

One of the main goals of studies of volcanic suites erupted in continental settings is to provide constraints on the crustal contribution to magma compositions (e.g. De Paolo, 1981; Hildreth & Moorbath, 1988). Assimilation of crustal rocks is able to produce extensive geochemical and isotopic modifications of mantle-derived melts, making recognition of pristine geochemical composition a difficult task. The problem is particularly challenging in active continental margins, where interaction between crustal and mantle

*Corresponding author. E-mail: frezzottiml@unisi.it

LEGEND

- Epiclastic and beach deposits
- 6 — Lavas and pyroclastics
- 5 — Pyroclastic deposits / Lava flows
- 4 — Fossa Caldera pyroclastics and deposits from other centres
- 3 — Rhyolitic-latitic lavas and domes
- 2 — Lavas and pyroclastics filling in Piano Caldera
- 1 — Lavas and pyroclastics of Primordial Vulcano
- Crater rims
- ○ Sampling locations

15°00'00" E

N

1 km

Scoglio di Capo Secco
Vulcanello
M. Minico
Lentia
La Fossa Cone
Il Piano
Spiaggia Lunga
Sponda Lena

38°22'00" N

ITALY
Tyrrhenian Sea
Sicily

Stromboli
Filicudi
Salina
Alicudi
Lipari
Vulcano
Panarea

(a)

(b)

Aeolian Arc
Capo d'Orlando
Messina
IONIAN SEA
Taormina
Etna

0   15   30
km

LEGEND

1 — 4 — 7
2 — 5 — 8
3 — 6 — 9

○ Sampling locations

components can occur both during magma ascent to the surface (wall-rock assimilation) and during subduction processes by addition of upper-crustal material to the mantle wedge (source contamination) (Hildreth & Moorbath, 1988; Vroon *et al.*, 1993; Patino *et al.*, 2000; Turner & Foden, 2001).

The Aeolian arc is a paradigm locality in which to study the role of crustal contamination in arc magmas. This archipelago is founded on 18–25 km thick continental crust belonging to the Calabro-Peloritano basement, which consists largely of metasedimentary and metaigneous rocks (Schenk, 1984; Rottura *et al.*, 1991; Van Dijk & Scheepers, 1995). According to several researchers, subduction of oceanic lithosphere is taking place, at least below the eastern part of the arc, as indicated by the occurrence of deep focus earthquakes (Faccenna *et al.*, 1997; Falsaperla *et al.*, 1999). The erupted volcanic rocks have calc-alkaline (CA), high-K calc-alkaline (HKCA), shoshonitic (SHO) and potassic alkaline (KS) compositions, which are closely associated in time and space (e.g. De Astis *et al.*, 1997, 2000, and references therein). These magmas show variable enrichments in incompatible trace element (ITE) and isotopic signatures; the latter range from typical mantle ratios in some primitive CA rocks, to values that are intermediate between crust and mantle. Therefore, isotopic variations highlight a role for both crustal and mantle source components in the genesis of Aeolian arc magmas (e.g. Ellam *et al.*, 1988, 1989; Ellam & Harmon, 1990; De Astis *et al.*, 1997, 2000).

There is, however, debate on the relative roles of wallrock contamination vs source contamination processes. Such a controversy, which applies to most, if not all, the volcanic suites erupted at active continental margins, requires further study. The evaluation of magma–wallrock interaction is hampered by the difficulty in assessing the geochemical composition of contaminants. Bulk rocks from the Calabro-Peloritano basement or xenoliths entrained in the lavas and pyroclastics have been used as the contaminants in models of magma assimilation in the Aeolian arc (e.g. Ellam *et al.*, 1988; Ellam & Harmon 1990; Esperança *et al.*, 1992; De Astis *et al.*, 1997, 2000). Crustal assimilation, however, may be selective, thus making bulk-rock compositions unsuitable for modelling contaminant

end-members; in addition, the xenoliths mostly represent restitic material, whose composition has been greatly modified by interaction with the host magma (e.g. Peccerillo & Wu, 1992).

A major step towards a better understanding of the assimilation process is to study the melts produced in the crust during partial melting. In crustal xenoliths, silicate melts trapped as inclusions may preserve melts produced during anatexis. Theoretically, each inclusion represents a snapshot of the liquid at a specific time, hence potentially recording the evolution of the melt; studies of inclusions, therefore, allow a reconstruction of the processes of melt extraction and migration, and provide a reliable determination of the compositional characteristics of the crustal contaminants.

The lavas and pyroclastic deposits of the Aeolian volcanoes contain abundant quartz-rich xenoliths (e.g. Honnorez & Keller, 1968; Peccerillo & Wu, 1992), and melt inclusions occur in the quartz crystals. These melt inclusions are considered representative of the composition of melts produced during anatexis of the basement rocks beneath the Aeolian arc. As a step towards developing a better insight into the processes of crustal melting, the nature of the quartz xenoliths, and the role of magma assimilation processes, we have investigated silicate-melt inclusions in quartz xenoliths occurring in the HKCA, SHO and KS lavas of the island of Vulcano. This island has been chosen because of the abundance of xenoliths and the occurrence of a wide variety of magmatic rock types from HKCA to KS and from mafic to silicic, which allows the role of contamination in the petrogenesis of the various types of magmas to be fully explored.

VOLCANOLOGICAL BACKGROUND

Vulcano is a complex volcanic edifice, located in a NNW–SSE-trending graben-like structure, which extends towards Lipari and Salina, parallel to the Tindari–Letoianni fault (Fig. 1a). It consists of pyroclastic successions and lavas that range from HKCA to KS (Keller, 1980; De Astis *et al.*, 1997). Volcanological studies indicate that volcanism started 120 kyr ago and migrated from SSE to NNW, forming four main eruptive centres (Primordial Vulcano, Lentia–Mastro

Fig. 1 (opposite). (a) Schematic map of Vulcano Island showing the volcanic rocks belonging to the six volcanic cycles, simplified from De Astis *et al.* (1997). Numbers refer to distinct eruptive cycles: 1, Primordial Volcano (120 ka); 2, Piano Caldera (99–20 ka); 3, Lentia–Mastro Minico; 4, La Fossa Caldera (15–8 ka); 5, La Fossa Cone (6 ka–present); 6, Vulcanello (183 BC–AD 1550). (b) Simplified geological map of the southern part of the Calabro-Peloritano basement from Bonardi *et al.* (1988). 1, Terrigenous and marine deposits (Pliocene–Pleistocene); 2, continental deposits (Pleistocene); 3, Stilo and Capo D'Orlando Flysch; 4, Longi Taormina sedimentary units (Paleocene); 5, sedimentary units (Cretaceous); 6, Maghrebian sedimentary units (Cretaceous); Aspromonte and Peloritani metamorphic units (granites, gneisses, amphibolites: Hercynian); 8, Stilo metamorphic units (granites and granodiorites: Permian–Carboniferous; gneisses, amphibolites, granulites: Alpine); 9, Polia Copaello metamorphic units (tonalites, granites, gneisses, amphibolites, marbles: pre-Hercynian); ○, sampling localities.

Minico complex, La Fossa Cone and Vulcanello) and two calderas (Piano and La Fossa calderas) (Keller, 1980; Castellet y Ballarà *et al.*, 1982; De Astis *et al.*, 1997).

Primordial Vulcano (120–100 ka) is a composite stratocone in the southernmost part of the island. It mostly consists of HKCA basalts and basaltic andesites, and some shoshonites. At about 99 ka, summit collapse formed the Piano caldera, which was subsequently almost completely filled by lava flows and scoria deposits (99–22 ka). The volcanics filling the Piano caldera show the same geochemical characteristics as those of Primordial Vulcano.

Between 28 and 13 ka, the Lentia–Mastro Minico volcanic activity started in the northwestern sector of the island; the erupted lavas and minor pyroclastites are predominantly HKCA rhyolites, and to a lesser extent, latites and HKCA dacites (De Astis *et al.*, 1997). The collapse of the Lentia–Mastro Minico volcanic complex gave rise to the western sector of La Fossa caldera, with the emission, between 15 and 8 kyr ago, of voluminous pyroclastic and lava flows from several centres, some of which were located offshore. These products display a wide range of compositional variation from shoshonite to trachyte.

From 6 ka to the present, the rhyolitic edifice of the La Fossa cone was formed in the centre of the La Fossa caldera. The dominant pyroclastic deposits and a few lava flows consist of shoshonitic rhyolites, displaying strong evidence of mingling with mafic melts. Since the eruption of AD 1888–1890, La Fossa cone has been in a high-temperature, fumarolic stage of activity.

Vulcanello formed as a separate island, probably in historical times. It consists of three or four pyroclastic cones aligned along an ENE–WSW direction, which rest upon a small shield composed of mafic potassic lavas. The last eruption of Vulcanello dates back to the 16th century, with the Valle del Roveto trachytic flow. The lavas from Vulcanello are shoshonites and latites (leucite-bearing tephrites; Keller, 1980) and, with the volcanic rocks from La Fossa cone, are amongst the most alkaline of the entire archipelago.

ANALYTICAL TECHNIQUES

Whole-rock analyses were performed on the quartz-rich xenoliths and on selected metamorphic rocks collected at various localities along the exposed Calabro-Peloritano basement on the adjacent mainland (Fig. 1b), which represent possible source rocks of the xenoliths. Major and trace element analyses were performed on powder pellets by X-ray fluorescence (XRF) at the Università di Perugia using a Philips PW 1400 X-ray fluorescence spectrometer. Correction for matrix effects was applied following Franzini &

Leoni (1972). The precision is better than 15% for V, Cr and Ni, better than 10% for Co, Cr, Y, Zr and Ba, and better than 5% for all the other elements. The accuracy has been tested on international standards and is better than 10%. FeO, Na_2O, MgO and LOI (loss on ignition) were determined by wet chemical analyses by atomic absorption spectrophotometry using DR-N, NIM-G, GSN, GA, BCR-1 and NIM-l international standards.

Eight samples were selected for detailed melt inclusion studies. Double polished, 100–200 μm thick wafers were prepared for microthermometric, electron microprobe, ion-probe and Raman microspectroscopic investigations. High-temperature microthermometric investigations were performed at the Vrije Universiteit, Amsterdam, using a high-temperature (up to 1600°C) heating–quenching stage developed by Sobolev & Slutskii (1984). Temperatures were measured by a Pt–Pt09Rh10 thermocouple, calibrated with gold, silver and synthetic compounds. Experiments were performed at 1 atm He, purified by a 700°C Ti filter (Sobolev & Danyushevsky, 1994). Heating times varied from 1 to 6 h as a result of the high viscosity of high-silica melts. Optimal heating rates of 2–5°C/min were used above 700–900°C and much lower rates (5–30°C/h) near homogenization. Measurement uncertainties were estimated to be ±5°C. Fast quenching (1–2 s) from homogenization temperatures was obtained by using a high gas flow. After quenching, the host minerals were mounted in epoxy and polished until the melt inclusions were exposed at the surface.

Electron microprobe analyses of minerals and glass contained in the inclusions were made using four-wavelength dispersive spectrometers on a JEOL JXA 8800 M Superprobe at the Vrije Universiteit, Amsterdam, using an acceleration voltage of 15 kV and a beam current of 25 nA. Spot sizes were 2–10 μm, with single-element counting times of 25–50 s on the peak and 10–25 s on the background. For the analyses of Mg, Al, Si, Ca and Fe the certified and well-tested JDF-D2#2 mid-ocean ridge basalt (MORB) standard glass from the Lamont–Doherty Earth Observatory, Columbia University, USA, was utilized. Jadeite and orthoclase were utilized as standards for Na and K, respectively. Alkali loss was minimized by measuring with a defocused spot of 2–10 μm, depending on the inclusion size, and measuring Na_2O first. The accuracy has been checked by incorporating at least five spots on each major element standard.

Secondary ionization mass spectroscopy (SIMS) investigations of the glasses were performed using a Cameca IMF 4F ion-probe at the Centro di Studio per la Cristallochimica e la Cristallografia, CNR Pavia. Analytical conditions were an acceleration

voltage of $12.5 kV$ and a beam current of $10 nA$; the composition of the incident beam was $^{16}O^-$. Natural international standard Kakanui kaersutite and Kakanui augite were utilized as standards (Mason & Allen, 1973; Czamanske *et al.*, 1993). Accuracy better than 10% was tested by analysing the standard glass NIST 610 and matching the results with average data from Pearce *et al.* (1997). Estimated errors are less than 10%.

Raman analyses of fluid and melt inclusions were carried out at the Università di Siena with a Jobin–Yvon confocal Labram multichannel spectrometer. Raman spectra were excited by an Ar^+ ion laser ($\lambda = 514.5 nm$), and scattering intensity was collected with a Peltier-cooled charge-coupled device (CCD) detector. The beam was focused to a spot size of about $1–2 \mu m$ using an Olympus $100\times$ lens. The scattered light was analysed using a Notch holographic filter with a spectral resolution of $1.5 cm^{-1}$ and a grating of 1800 grooves/mm (Frezzotti, 2001*a*).

RESULTS

Quartz xenoliths

Xenoliths of crustal rocks are commonly observed in the lavas and pyroclastic rocks from Vulcano and the other Aeolian Islands. Metamorphic xenoliths show a range of compositions and textures; most are quartz grain aggregates, but minor metapelites, vesuvianite- and grossular-bearing skarns, and cordierite- and sillimanite-bearing gneisses also occur (Honnorez & Keller, 1968; Barker, 1987; Peccerillo & Wu, 1992). Magmatic xenoliths consist of gabbros, diorites and lavas. Rare ultramafic xenoliths consisting of cumulate-textured clinopyroxene, olivine and Ti-magnetite are also present (Peccerillo & Wu, 1992; Peccerillo *et al.*, 1993).

All of the studied samples are quartz-rich xenoliths. These have been collected from lavas and pyroclastic units of well-known chemical composition and stratigraphic position from Vulcano Island (De Astis *et al.*, 1997, 2000). Sampled sequences (10–15 samples for each locality) include the Primordial Vulcano HKCA basaltic-andesite lavas of Sponda Lena, the HKCA dacites of Scoglio di Capo Secco and Mastro Minico, belonging to the Lentia–Mastro Minico complex, and the Vulcanello leucite tephrites (Fig. 1a).

The quartz-rich xenoliths generally have angular shapes, and range in size from a few centimetres up to $10 cm$ (Fig. 2a); typically they are white, which makes them easy to distinguish in the outcrops. Contacts with the host lavas are sharp but locally the xenoliths appear to have disaggregated within the host melt. The xenoliths consist mostly of quartz (>98%

modal), with subordinate amounts of K-feldspar and/or orthopyroxene and plagioclase. Zircon, apatite and titanite grains occur in some xenoliths. Textures are granular (Fig. 2b) and all the xenolith samples contain significant quantities of colourless glass, both as films along the grain boundaries and as silicate-melt inclusions within single quartz grains (Fig. 2b and c).

Based on the microstructural characteristics of quartz, two types of grains can be distinguished, which coexist in the same xenolith. The first, 'Q_1' grains (from < 100 to $600 \mu m$), show rounded or spongy outlines, are always surrounded by films of clear glass and contain silicate melt inclusions $\pm CO_2$ fluid inclusions (Fig. 2b and c); in many Q_1 quartz grains, at the contact with the glass, a rim of a few tens of μm of cristobalite has been identified by Raman spectroscopy (Fig. 2d). The second type of quartz grains, 'Q_2', consist of polygonal grains (from 100 to $800 \mu m$) bounded by faces that intersect at 120° forming a polygonal aggregate microstructure (Fig. 2e). Abundant CO_2 fluid inclusions are present in Q_2, but melt inclusions are conspicuously absent (Fig. 2f).

Clear glass occurs as intergranular veinlets between 100 and $200 \mu m$ across, along Q_1 grain boundaries, and as thin films (up to $50 \mu m$) filling small fractures and forming short trails or clusters of silicate-melt inclusions in Q_1 grains. The veinlets are evenly distributed and form a branching network that encloses Q_1 grains, suggesting that the melt may have migrated along grain boundaries and microfractures (Fig. 2b). The glass is variably devitrified and microcrystals of feldspars are commonly present along with several rounded voids. Overall, the glass microstructures indicate rapid quenching and suggest that the veins represent an open system that re-equilibrated to very low-pressure conditions.

Most xenoliths are cut by veinlets of glassy or microcrystalline material emanating from the enclosing host volcanic rocks. Glass from the host lava is distinguished petrographically from the intergranular films and inclusions on the basis of its brown–yellowish colour. Veinlets of host lavas were carefully discarded during powder preparation for whole-rock xenolith analyses. However, because of the difficulty of avoiding contamination with the host-rock, a sufficient and representative amount of powder was obtained only for two samples. Their composition is reported in Table 1.

Xenoliths are very rich in silica and contain only small amounts of other major elements. Incompatible trace element patterns show that the xenoliths are depleted in all the incompatible elements by more than an order of magnitude with respect to the quartz-rich metamorphic rocks from the Calabro-Peloritano basement (Fig. 3).
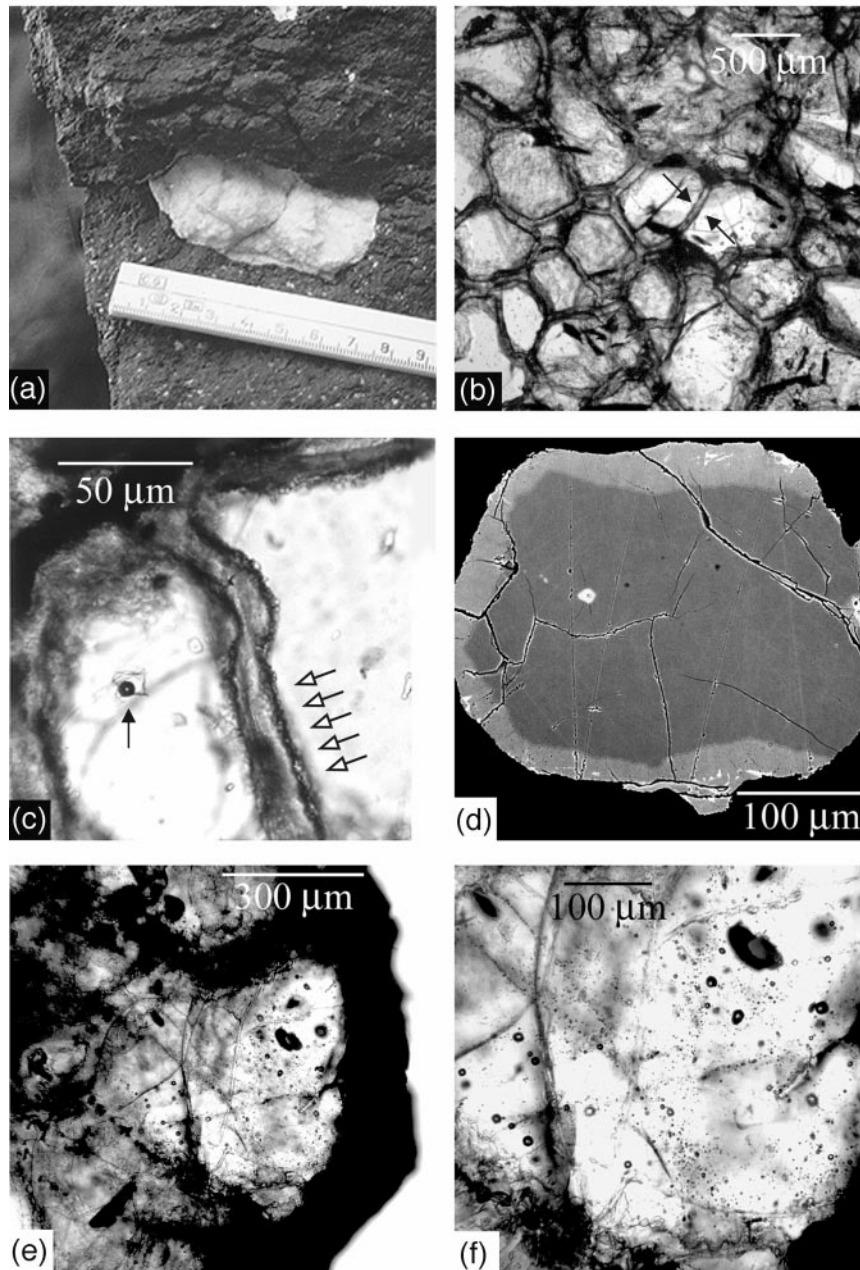
Fig. 2. Photomicrographs of the studied quartz xenoliths (plane-polarized light unless otherwise indicated). (a) Large quartz xenolith in lavas from Vulcanello. (b) Q_1 grain microstructures in a quartz xenolith from Sponda Lena (sample Vu.SL). Relic Q_1 grains are surrounded by rims of rhyolitic glass (arrows). (c) Typical association of high-silica melt inclusions in a Q_1 grain from Sponda Lena quartz xenolith (sample Eo.98.23). The distribution of inclusions close to grain boundaries (black arrow), which are lined and separated by a film of colourless glass (white arrows), should be noted. The inclusions resulted from infiltration of high-silica melt in the quartz crystals. (d) A single Q_1 quartz grain (dark grey) surrounded by a rim of cristobalite (light grey). SEM backscattered microphotograph (sample Eo.98.22). (e) Q_2 grains containing abundant fluid inclusions in quartz xenolith from Vulcanello. It should be noted that melt inclusions are absent (sample Eo.98.22). (f) Detail of (e) showing CO_2 inclusions in a Q_2 grain. Most fluid inclusions are vapour dominated at room temperature.

Metamorphic rocks of the Calabro-Peloritano basement

The Calabro-Peloritano metamorphic belt is composed of Hercynian metasedimentary, metaigneous and igneous rocks partially overlain by Mesozoic and Cenozoic ophiolite and sedimentary sequences (e.g. Schenk, 1984; Rottura *et al.*, 1991). The metamorphic rocks have a wide range of metamorphic grades and textures and include phyllites, mica schists, gneisses, migmatites, amphibolites and granulites (Fig. 1b). For the

Table 1: Representative whole-rock chemical analyses of quartz xenoliths and of metamorphic rocks of the Calabro-Peloritano basement

	Quartz xenoliths			Metamorphic rocks of the Calabro-Peloritano basement								
	Eo9821	Vugea		PE 1	PE 1a	PE 1b	PE 2a	PE 2c II	PE 3b	PE 4	PE 5a	PE 6a
wt %			*wt* %									
SiO₂	98·17	99·26	SiO₂	71·95	70·04	70·12	69·87	64·29	66·94	62·33	69·58	67·08
TiO₂	0·01	0	TiO₂	0·18	0·64	0·09	0·75	0·92	0·23	0·84	0·36	0·52
Al₂O₃	0·84	0·47	Al₂O₃	15·67	13·96	15·6	12·94	14·3	21·12	18·14	14·92	17·62
Fe₂O₃	0·12	0·05	Fe₂O₃	1·39	2·2	0·69	2·79	3·38	0·82	4·65	2·08	3·59
FeO	0·03	0	FeO	0·52	1·52	0·03	2·41	3·78	0·2	1·42	1·34	0·08
MnO	0·04	0·04	MnO	0·03	0·05	0·01	0·04	0·09	0·04	0·04	0·04	0·03
MgO	0·03	0·02	MgO	0·48	1·04	0·14	2·62	2·62	0·23	1·94	1·71	0·94
CaO	0·07	0·05	CaO	1·77	1·39	0·78	1·17	1·72	1·61	0·85	2·82	0·7
Na₂O	0·11	0·04	Na₂O	3·54	3·03	2·85	3·28	2·74	4·08	2·33	4·24	3·09
K₂O	0·16	0·03	K₂O	3·41	5·21	8·86	2·46	4·35	3·15	4·18	1·84	3·99
P₂O₅	0·01	0	P₂O₅	0·12	0·12	0·31	0·13	0·19	0·25	0·18	0·06	0·1
LOI	0·41	0·03	LOI	0·94	0·8	0·51	1·55	1·62	1·33	3·1	1·01	2·26
ppm			*ppm*									
V	8	0	Ba	822	764	734	1050	422	562	665	413	599
Cr	3	1	Rb	113	174	104	107	235	54	154	65	154
Co	1	0	Sr	343	135	120	169	104	164	140	387	157
Ni	0	0	Y	0	21	38	14	26	19	18	11	5
Cu	39	0	Zr	87	165	29	177	162	24	222	79	123
Zn	8	6	Nb	11	14	4	12	17	13	23	6	10
Ga	2	0	Ni	8	10	7	21	23	8	18	18	14
Rb	6	2	Cr	17	31	8	76	93	10	69	48	36
Sr	6	0	V	10	57	8	106	132	3	100	58	54
Y	3	0	La	32	24	12	25	49	12	35	10	26
Zr	6	2	Ce	51	51	22	49	80	18	73	29	49
Nb	0	0										
Ba	4	0										
La	6	0										
Pb	17	14										
Ce	3	0										
Th	12	12										

	Metamorphic rocks of the Calabro-Peloritano basement											
	PE 6b	PE 7	PE 9	PE 10b	PE 11	PE 12	PE 16	PE 18	PE 19	PE 20a	PE 21a	PE 22
wt %												
SiO₂	60·69	83·15	72·16	99·55	75·68	67·62	67·09	71·49	67	65·38	74·46	73·57
TiO₂	1·3	0·45	0·41	0·01	0·65	0·41	0·76	0·11	0·97	0·35	0·28	0·55
Al₂O₃	16·52	9·28	13·56	0·12	13·79	15·79	14·55	16·11	15·74	17·67	12·3	13·11
Fe₂O₃	7·64	2·18	1·77	0·08	3·13	2·87	5·66	1·38	6·89	2·19	4·38	5·44
FeO	0·06	0·08	0·39	0	0	0	0	0	0	0	0	0
MnO	0·09	0·02	0·03	0	0·03	0·04	0·06	0·02	0·05	0·02	0·06	0·07
MgO	0·82	0·27	0·24	0·01	0·47	2·81	1·62	2·59	2·18	1·43	0·82	1·99
CaO	4·22	0·17	1·26	0·03	0·17	0·61	3·42	0·61	0·68	4·96	3·8	1·41

Table 1: continued

	PE 6b	PE 7	PE 9	PE 10b	PE 11	PE 12	PE 16	PE 18	PE 19	PE 20a	PE 21a	PE 22

Metamorphic rocks of the Calabro-Peloritano basement

|	PE 6b	PE 7	PE 9	PE 10b	PE 11	PE 12	PE 16	PE 18	PE 19	PE 20a	PE 21a	PE 22
Na_2O	3·23	1·46	3·88	0·05	2·08	1·51	2·47	2·83	1·18	4·35	3·3	0·32
K_2O	3·04	1·26	5·46	0·02	1·94	3·43	3·48	4·09	4·46	3·03	0·37	3·46
P_2O_5	0·22	0·08	0·1	0·01	0·08	0·1	0·19	0·06	0·03	0·04	0·08	0·08
LOI	2·17	1·6	0·74	0·12	1·99	4·81	0·71	0·71	0·84	0·58	0·15	0
ppm												
Ba	626	140	1302	1	348	883	1727	620	652	819	233	965
Rb	184	52	84	3	65	137	98	90	161	101	4	59
Sr	201	44	322	0	133	140	253	161	77	796	192	280
Y	15	19	3	0	26	27	3	16	20	0	20	28
Zr	175	598	28	0	980	130	217	130	208	100	60	213
Nb	13	9	11	65	15	21	13	10	25	0	0	11
Ni	15	14	8	6	16	12	8	8	23	8	11	9
Cr	34	39	9	8	42	115	21	24	93	24	16	74
V	52	51	2	1	61	190	81	130	130	37	28	86
La	25	27	12	0	38	50	53	34	38	52	5	35
Ce	54	60	15	0	67	100	101	51	63	95	26	68
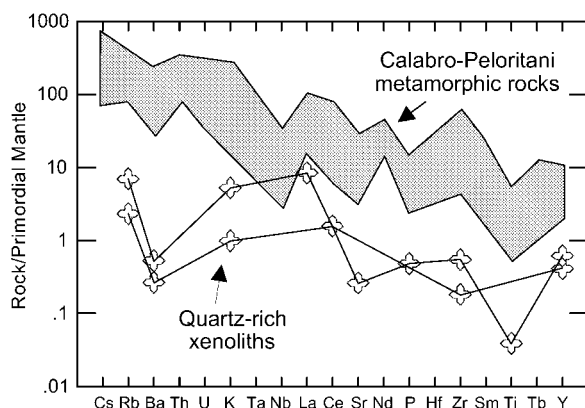
Fig. 3. Primordial mantle normalized incompatible trace element patterns for the sampled metamorphic rocks from the Calabro-Peloritano basement and for the two analysed quartz-rich xenoliths. Normalization constants from Wood *et al.* (1979).

purpose of the present study, sampling was concentrated on the quartz-rich rocks, as they may represent the potential protoliths of the quartz-rich xenoliths entrained in the Aeolian volcanics. The samples selected for this study include gneisses, mica schists, granulites and migmatites. Gneisses and schists have typical lepidoblastic textures and consist mainly of quartz, K-feldspar and plagioclase with subordinate and variable amounts of biotite and muscovite; apatite, zircon and epidote occur as accessory phases. Garnet is abundant in some schists, and minor sillimanite is

occasionally observed. Granulites show heteroblastic textures and consist of dominant quartz, K-feldspar and plagioclase, variable amounts of garnet, minor sillimanite, biotite and amphibole, and accessory zircon, apatite, monazite and epidote. Migmatites have medium- to coarse-grained granoblastic textures and consist of quartz, K-feldspar and plagioclase, biotite and muscovite; zircon, apatite and epidote are present in accessory amounts.

Major and trace element compositions have been obtained to provide data for interpreting the significance of the melt inclusions and to test the assimilation processes that may have occurred in the Aeolian magma (Table 1).

Silica-rich glasses

Petrography

Glasses, which occur as intergranular films and as inclusions in Q_1 quartz grains, have high-silica contents and resemble rhyolites. The compositional affinity and physical continuity between the glasses occurring as intergranular films and glasses forming the melt inclusions suggest a close genetic relationship (Fig. 4a). Because late, low-pressure crystallization products, probably associated with fluid degassing, were recognized in interstitial glasses, the present study focuses on melts (glasses) trapped as inclusions.

It is widely accepted that closed-system melt inclusions preserve the geochemical signature of the trapped
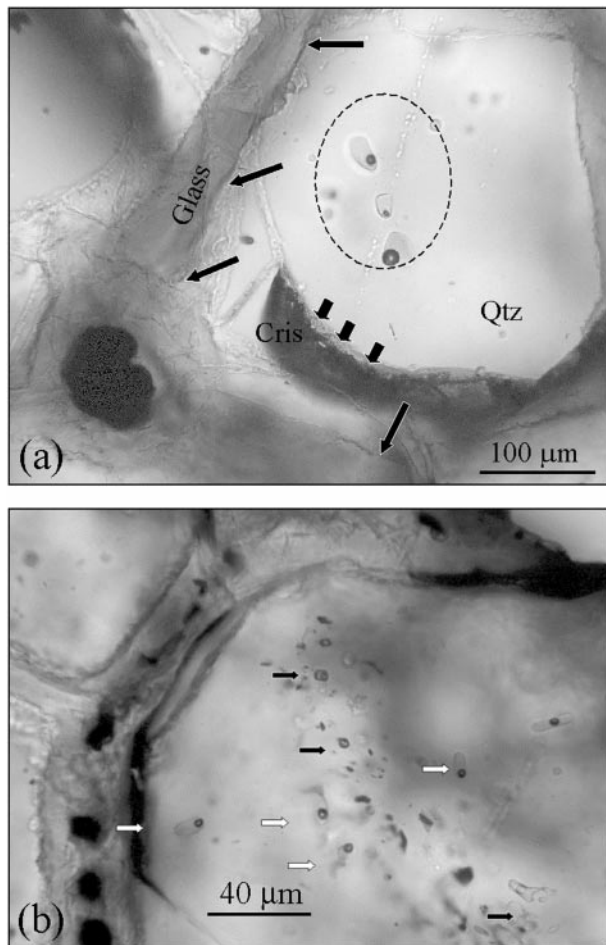
Fig. 4. Microstructural characteristics of glass in quartz xenoliths. (a) Colourless high-silica glass present as micro-veins and melt inclusions in a Q_1 grain. Large early melt inclusions are present in the internal part of the grain. (Note the presence of the cristobalite rim.) Cris, cristobalite; Qtz, quartz. (b) Late trail of melt inclusions (white arrows) coexisting with high-density CO_2 inclusions (black arrows).

melts better than open-system microveins, as decompression and cooling of the host xenoliths during eruption may cause the vein melts to partially crystallize at low pressure, which will modify their original composition (e.g. Schiano & Bourdon, 1999; Sobolev *et al.*, 2000). Such processes, which can generate strong geochemical modifications of melts (glasses) present in the veins, may be reversed during rehomogenization experiments in silicate-melt inclusions, restoring the original melt composition (Frezzotti, 2001*b*).

Clear glass, trapped as silicate-melt inclusions (usually <20 μm, and rarely up to 50 μm) in Q_1 grains, occurs in clusters and/or as short trails originating at grain boundaries (i.e. secondary inclusions; Fig. 4). Although inclusions are associated with a single melt-trapping event, a relative trapping order can be deduced between inclusions, based on their

distribution within the quartz host. Early-trapped inclusions are present in the inner parts of the Q_1 grains (encircled area in Fig. 4a), whereas late-trapped inclusions are found in the outer parts, often contained within the cristobalite rim to Q_1 (white arrows in Fig. 4b). Both early and late inclusions have similar characteristics. They have rounded morphologies commonly reaching negative crystal shapes and usually contain colourless glass and a bubble (Fig. 4a). Inclusions consisting only of glass are also present. In some inclusions, a small shrinkage bubble is present, but typically they contain immiscible CO_2, which can be present either as a low-density gas bubble (detected by Raman spectroscopy) or as a high-density fluid (Fig. 4b). In this last case, the presence of abundant, high-density, pure CO_2 fluid inclusions indicates that the system was volatile rich and CO_2 oversaturated at some stage [heterogeneous trapping of silicate melt (white arrows) and fluids (black arrows), Fig. 4b]. Although daughter minerals are absent, single crystals of wollastonite, or orthopyroxene, clinopyroxene, quartz, feldspar, sulphide or oxide, are infrequently observed within melt inclusions.

Chemical composition

Some 70 quenched silicate-melt inclusions in quartz grains from quartz xenoliths from Vulcano were analysed for major elements, Cl, F and S. The major element compositions are reported in Table 2. In general, the glasses have variable compositions but all are rich in silica and potassium (4·2–6·2 wt % K_2O; 72–81 wt % SiO_2), and resemble high-K rhyolites (Fig. 5). Most compositions are peraluminous with alumina saturation index [ASI: $Al_2O_3/(K_2O + Na_2O + CaO)$] up to 1·35. High contents of chlorine (up to 8000 ppm) were measured. Microprobe analyses have totals between 95 and 100 wt %, suggesting that the glasses have variable water contents. Qualitative Raman observations on the glass confirm the presence of water, with a well-developed band centred at 3550 cm^{-1} (not shown). Comparison of glass compositions with those of the lavas and pyroclastics from Vulcano is shown in Fig. 5. All oxides have been recalculated on a water-free basis. The analysed inclusions have similar K_2O contents to the most differentiated volcanics from Vulcano, but have higher silica contents.

Variation diagrams of major elements vs CaO are shown in Fig. 6. The analysed melt inclusions show a scattered distribution; however, a rough positive correlation of CaO vs MgO and negative correlations for SiO_2, K_2O and Al_2O_3 can be recognized. Compared with the quartz-rich metamorphic rocks of the Calabro-Peloritano basement (grey areas in Fig. 6), the analysed inclusions have higher SiO_2, and slightly

Table 2: Representative electron-microprobe analyses of glass in quenched melt inclusions in the quartz xenoliths

Cycle:	S.Lena	S.Lena	S.Lena	S.Lena	S.Lena	S.Lena	S.Lena	S.Lena	S.Lena	S.Lena	S.Lena	S.Lena	S.Lena
n:	3a-1	3c-2	9a-2	10a-1	10c-2	11b-2	12a-1	15a-1	16a-1	44b	45	46	16b
T_h (°C):	1080	1080	1100	1092	1092	1100	1084	1130	1070	1080	1070	1100	1070
t:	L	E	L	E	E	L	L	E	E	L	E	E	E
SiO_2	75·84	76·85	74·09	75·73	74·92	75·78	76·6	79·29	76·94	77·4	78·1	77·8	77·42
TiO_2	0	0	0	0	0	0·05	0	0·37	0·27	0·34	0·26	0·39	0·36
Al_2O_3	8·17	8·02	7·71	7·72	8·25	8·61	7·82	10·97	11·5	10·2	9·69	10·2	10·55
Fe_2O_3	1·48	1·29	1·53	1·71	1·19	1·21	1·37	0·18	0·11	0·1	0·29	0·19	0·12
FeO	2·97	2·59	3·05	3·42	2·39	2·42	2·73	0·36	0·21	0·2	0·59	0·37	0·24
MgO	0·45	0·42	0·38	0·59	0·33	0·24	0·33	0·14	0·12	0·1	0·16	0·14	0·12
CaO	2·53	2·98	4·77	2·94	4·23	4·16	3·18	0·73	0·91	0·49	0·56	0·61	0·72
Na_2O	2·05	2·67	2·4	2·4	2·3	1·9	2·07	2·12	2·42	1·47	1·63	1·4	2·16
K_2O	4·83	4·71	4·51	4·57	4·64	4·42	4·85	5·94	6·04	6·17	5·64	5·79	5·67
Cl	0·49	0·46	0·46	0·64	0·78	0·27	0·53	0·17	0·28	0·03	0·05	0·15	0·11
Total	98·81	99·99	98·9	99·72	99·03	99·06	99·48	100·27	98·8	96·5	96·97	97·04	97·47
Cycle:	Lentia	Lentia	Lentia	Vulc.	Vulc.	Vulc.	Vulc.	Vulc.	Vulc.	Vulc.	Vulc.	Vulc.	Vulc.
n:	19a	19b	19c	28a	28b-1	30a-1	31a	32a	32c	32d	33a	34a-1	34a-2
T_h (°C):	980	980	980	1100	1100	1100	1100	1100	1100	1100	1100	1100	1100
t:	L	L	L	L	E	E	E	L	L	L	L	E	E
SiO_2	75·80	77·99	77·59	81·10	75·90	78·50	78·70	77·20	74·80	75·90	78·80	76·40	78·90
TiO_2	0·11	0·12	0·11	0·09	0·00	0·01	0·07	0·10	0·10	0·07	0·02	0·03	0·00
Al_2O_3	11·19	9·91	10·84	10·30	11·80	9·56	10·00	6·98	7·54	6·34	11·80	11·40	10·20
Fe_2O_3	0·79	0·74	0·77	0·21	0·06	0·32	0·27	1·61	1·47	1·80	0·13	0·07	0·06
FeO	1·59	1·48	1·54	0·43	0·13	0·65	0·55	3·23	2·93	3·59	0·27	0·14	0·11
MgO	0·20	0·15	0·17	0·05	0·28	0·10	0·08	0·55	0·55	0·73	0·28	0·17	0·19
CaO	0·52	0·51	0·42	0·32	2·02	0·33	0·29	0·99	1·41	1·71	2·50	2·00	1·08
Na_2O	2·43	2·42	2·36	0·71	1·24	1·28	1·06	1·48	1·41	1·32	0·98	0·70	1·22
K_2O	5·09	4·67	4·93	5·37	3·58	5·73	6·02	5·70	6·04	5·68	3·29	3·65	3·56
Cl	0·21	0·18	0·17	0·02	0·22	0·18	0·05	0·18	0·49	0·59	0·13	0·26	0·20
Total	97·93	98·17	98·90	98·60	95·23	96·66	97·09	98·02	96·74	97·73	98·20	94·82	95·52

For each analysis, the volcanic cycle, the temperature of homogenization and the relative timing of trapping are indicated. n, inclusion number; T_h, homogenization temperature; t, relative time of trapping; E, early trapped inclusion; L, late trapped inclusion; Vulc., Vulcanello.
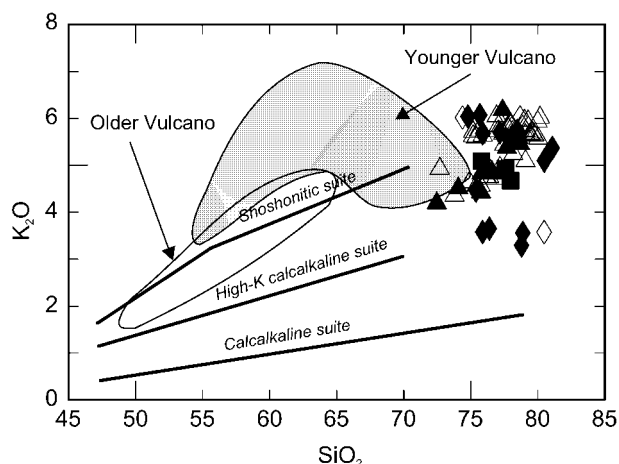
Fig. 5. SiO_2 vs K_2O (Peccerillo & Taylor, 1976) for melt inclusions and Vulcano acid rocks (grey shaded field). Triangles, Sponda Lena; squares, Lentia; diamonds, Vulcanello. Open and filled symbols indicate early and late trapped inclusions, respectively. Compositions of lavas at Vulcano are indicated by the shaded areas.

higher K_2O and K_2O/FeO_{total}, comparable CaO and Na_2O, and lower MgO, FeO_t, Al_2O_3 and TiO_2. In general, late inclusions (filled symbols in Fig. 6) and early inclusions (open symbols in Fig. 6) have comparable compositions.

Table 3 summarizes the ion-microprobe abundances of trace elements in the silicate-melt inclusions. Data are available for Sponda Lena and Vulcanello only, as the inclusions from Lentia-Mastro Minico are too small to be analysed. Mantle-normalized, trace element patterns for the melt inclusions show large variations in trace element abundance (Fig. 7). At Sponda Lena two groups of compositions can be recognized. The first group (open triangles in Fig. 7) is characterized by strong depletion in some incompatible trace elements (ITE), especially REE, Zr, Ba and Y, but moderate or no depletion in Rb, K, Sr and Ti, which have abundances close to the quartz-rich metamorphic rocks from Calabro-Peloritano basement. A second group of inclusions (filled triangles in Fig. 7) have ITE patterns that closely resemble the metamorphic rocks from the basement. Detailed petrographic studies indicate that ITE-depleted patterns belong to the internal, early-trapped inclusions, whereas the ITE-enriched compositions are typical of late-trapped inclusions occurring in the outer parts of the quartz grains. The melt inclusions from Vulcanello show a smaller range of variation than the Sponda Lena inclusions, but can be still divided into two groups on the basis of both their incompatible element depletion and their relative time of entrapment. However, the early-trapped inclusions (open diamonds, Fig. 7) at Vulcanello are much less depleted (especially in Cs, Rb and Ba) than those from Sponda Lena.

Chondrite-normalized REE patterns (Fig. 8) show large variations in REE abundance. Early ITE-depleted glasses (open symbols in Fig. 8) are characterized by low light REE (LREE) contents, mostly below detection limits, which result in flat unfractionated patterns, generally with a strong positive Eu anomaly. Late ITE-enriched glasses have higher REE abundances with LREE enrichment resulting in fractionated patterns that have negative, or no Eu anomalies (filled symbols). These latter patterns closely resemble the analysed metamorphic rocks of the Calabro-Peloritano basement (grey area in Fig. 8).

Temperatures and pressures of trapping of the silica-rich melts

High-temperature microthermometric heating–quenching experiments were performed on the inclusions in quartz for all the studied xenoliths to rehomogenize the glasses in the inclusions and to obtain the temperature of homogenization (T_h). This is determined by the complete disappearance of any bubbles and corresponds to the temperature at which the rhyolitic melts were trapped as inclusions in their host quartz. Melt inclusions require some preliminary selection, as they commonly have CO_2 fluids within the bubble, either of high density (coexisting liquid and vapour CO_2) or of low density (CO_2 vapour only; detected by Raman spectroscopy), which is evidence for volatile oversaturation. For these reasons, all inclusions with relatively large bubbles were excluded; measurements were concentrated on those inclusions with only small shrinkage bubbles.

Temperatures of homogenization (T_h) range between 1060 and 1110°C ($\pm$5°C) for inclusions from xenoliths in the HKCA basaltic-andesite lavas of Sponda Lena and between 1000 and 1110°C ($\pm$5°C) for inclusions in the xenoliths from the leucite tephrites of Vulcanello. The single inclusion from a xenolith in the rhyolites of the Lentia–Mastro Minico complex yields a T_h of 980°C ($\pm$5°C), which is in agreement with homogenization temperatures measured by Clocchiatti *et al.* (1994) for melt inclusions from similar quartz-rich xenoliths in rhyolites from the La Fossa cone, which range between 930 and 1030°C. It should be noted that no differences in T_h were observed between the early ITE-depleted inclusions and the late ITE-enriched inclusions (see Tables 2 and 3).

Based on these data, we conclude that high-silica melts were trapped in the T interval 980–1100°C, with the highest T_h ($\approx$1100°C) recorded by inclusions from xenoliths found in lavas of more primitive composition. Based on melt thermometry, Zanon *et al.* (2003) obtained the following temperature ranges for the host lavas: 1060–1128°C for Sponda Lena lavas,
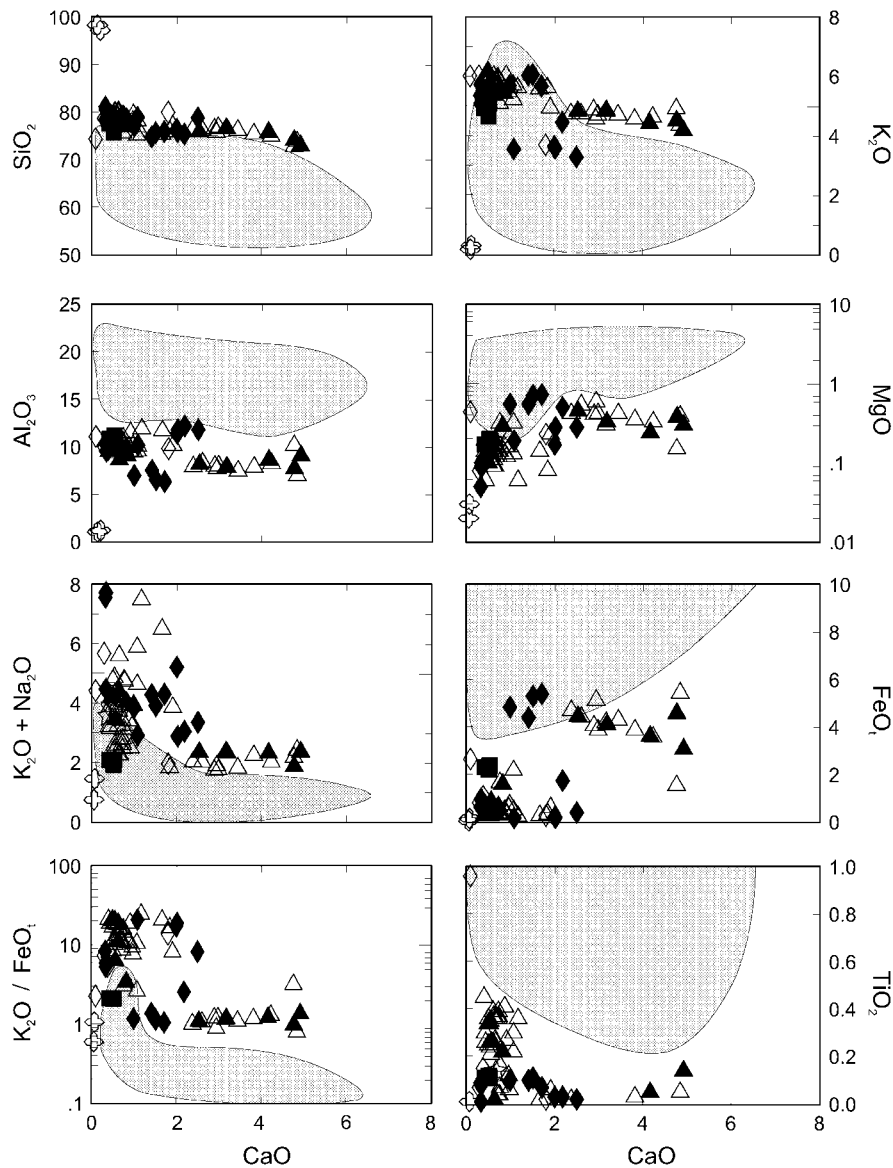
Fig. 6. Variation diagrams vs wt % CaO for the melt inclusions and for the Calabro-Peloritano metamorphic rocks (grey field). Open crosses, quartz-rich xenoliths; triangles, Sponda Lena; squares, Lentia; diamonds, Vulcanello. Open and filled symbols indicate early and late trapped inclusions, respectively (see text for explanation).

941–983°C for Lentia rhyolitic lavas, and 1086–1090°C for the lavas of Vulcanello [±7°C (Sisson & Grove, 1993), and ±40°C (Albarède, 1992)]. T_h values from melt inclusions in xenoliths, approximating lava temperatures, indicate that thermal equilibrium was achieved between the products of *in situ* melting of the basement xenoliths and the host lavas.

Because fluid inclusions often coexist with silicate-melt inclusions, it is possible to calculate the pressures of trapping of the rhyolitic melts by combining homogenization temperatures (T_h) of melt inclusions with the density of the fluid inclusions. Pressures obtained from the study of CO_2 inclusions indicate that the rhyolitic melts were trapped in the inclusions at relatively high pressures, corresponding to middle–lower-crustal depths (3·5–5·6 kbar; 14–21 km, Zanon *et al.*, 2003).

DISCUSSION

The main objectives of this study are to understand:

1. the origin of quartz-rich xenoliths;
2. the genesis of the silica-rich rhyolitic glasses in the melt inclusions and their record of crustal melting processes;

Table 3: *Representative chemical analyses of quenched melt inclusions in quartz xenoliths*

	S.Lena	S.Lena	S.Lena	S.Lena	S.Lena	S.Lena	S.Lena	S.Lena	Vulc.	Vulc.	Vulc.	Vulc.	Vulc.
T_h (°C):	1070	1105	1105	1105	1105	1100	1100	1087	1100	1100	110	1100	1100
n:	16c-1	17a	17b-1a	20a-1	20b-1	46-3	46-4	49-a	27b	30a-2	30a4m	32b	4b-1
t:	E	E	E	L	E	E	L	E	L	E	E	L	L
Spot (μm):	5	7	7	5	5	7	7	7	7	5	7	7	5
wt %													
SiO_2	75·92	78·53	79·77	72·97	72·70	78·00	78·70	79·60	80·50	78·90	74·40	75·70	75·40
TiO_2	0·00	0·26	0·21	0·14	0·00	0·30	0·22	0·26	0·08	0·15	0·96	0·11	0·03
Al_2O_3	12·62	10·23	9·80	9·06	10·17	9·90	9·12	9·66	10·40	9·70	11·10	6·52	12·20
FeO_{tot}	0·34	0·34	0·28	3·07	1·54	0·73	1·60	0·30	0·96	1·09	2·65	5·30	1·74
MgO	0·08	0·12	0·12	0·30	0·15	0·14	0·29	0·06	0·09	0·17	0·44	0·71	0·50
CaO	1·84	0·66	0·55	4·92	4·76	0·43	0·82	0·44	0·33	0·38	0·09	1·51	2·18
Na_2O	3·07	2·46	2·30	1·77	2·26	1·85	1·35	1·46	0·66	1·47	1·36	1·55	1·46
K_2O	5·63	5·58	5·64	4·19	4·92	5·86	5·45	5·70	5·10	5·82	6·02	6·07	4·46
Cl	0·01	0·09	0·12	0·25	0·02	0·06	0·01	0·07	0·01	0·10	0·30	0·32	0·01
Total	99·51	98·27	98·79	96·67	96·52	97·27	97·56	97·55	98·13	97·78	97·32	97·79	97·98
ASI	1·2	1·18	1·15	0·83	0·85	1·22	1·2	1·27	1·71	1·26	1·49	0·71	1·51
ppm													
K			45446	37010			46310	41746	44552				
Sc	1	3				4	3	1			1		
Ti	5·3	1014	1431	1041	2·3	972	1559	1435	415	468	7326	552	76
V	0·94	1·3	1·4	5·3	0·5	5·6	51	3·9	4	0·6	11	32	25
Cr	0·3	0·4	0·4	1	0·2	0·1	1·7	0·3	0·6	0·3	1·9	1·1	0·9
Rb	37	87	116	142	120	76	208	103	79	115	190	139	185
Sr	141	16	27	104	194	13	110	26	29	35	7	196	76
Y	0·14	0·03	0·03	45·6	0·01	0·01	13	0·01	14·6	4·4	0·9	13·6	3
Zr	0·04	0·07	0·16	125		0·09	67	0·08	23	0·26	3·8	90	21
Nb		7·4	6·9	5·2	0·09	5·1	9·4	0·5	5·8	0·47	4·5	11	8·2
Cs	0·1	3·1	4·3	8·2	0·2	3·2	6·4	4·7	3·5	6	4·5	6·8	9·4
Ba	17	37	61	166	1·7	72	195	71	461	519	854	242	76
La	0·09			46·4	0·01	0·01	14	0·01	9·1	2	0·6	29·9	10·5
Ce	0·12	0·02	0·04	98·7		0·02	26·5		19·9	3·2	0·7	51·9	21·2
Nd	0·12	0·07		46·2			11		10·6	1·6	0·5	17·4	8·2
Sm	0·02	0·03	0·03	9·3	0·03		2·3		1·8	0·59	0·13	3	1·75
Eu	0·32		0·01	0·36	0·03		0·62			0·27	0·87	0·52	0·51
Gd	0·02	0·02	0·08	8·6			2·39		2·95	0·6	0·2	2·86	1·54
Dy	0·02	0·02	0·03	8·6	0·05	0·03	2·48	0·02	2·72	0·8	0·3	3	0·95
Er	0·05			4·7	0·03		1·46	0·03	1·3	0·5	0·2	1·76	0·13
Yb			0·03	4·6	0·02		1·27	0·02	1·64	0·3	0·08	1·85	0·2

Major elements by electron microprobe. Trace elements by SIMS. For each analysis the volcanic cycle, timing of trapping and temperature of homogenization are indicated. *n*, inclusion number; T_h, homogenization temperature; *t*, relative time of trapping; E, early trapped inclusion; L, late trapped inclusion; Vulc., Vulcanello; ASI, alumina saturation index [$Al_2O_3/(K_2O + Na_2O + CaO)$].
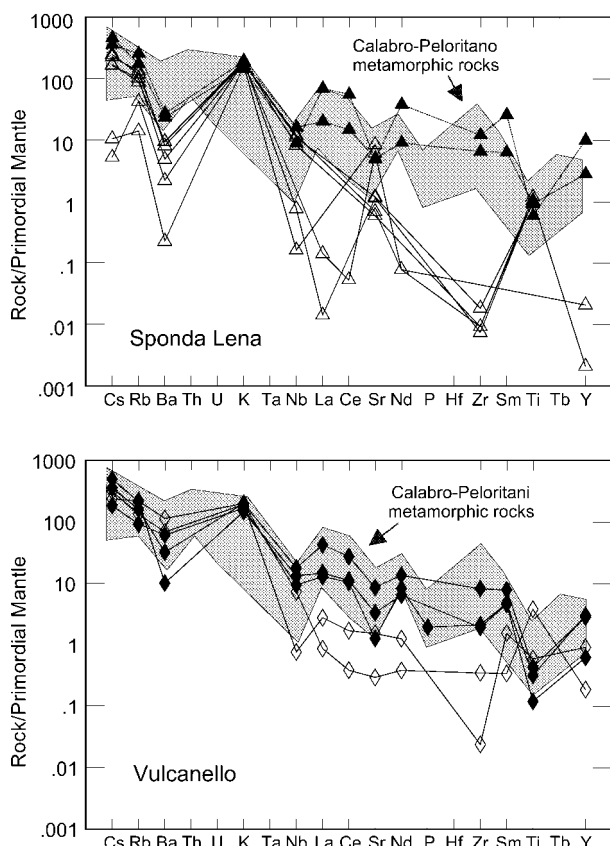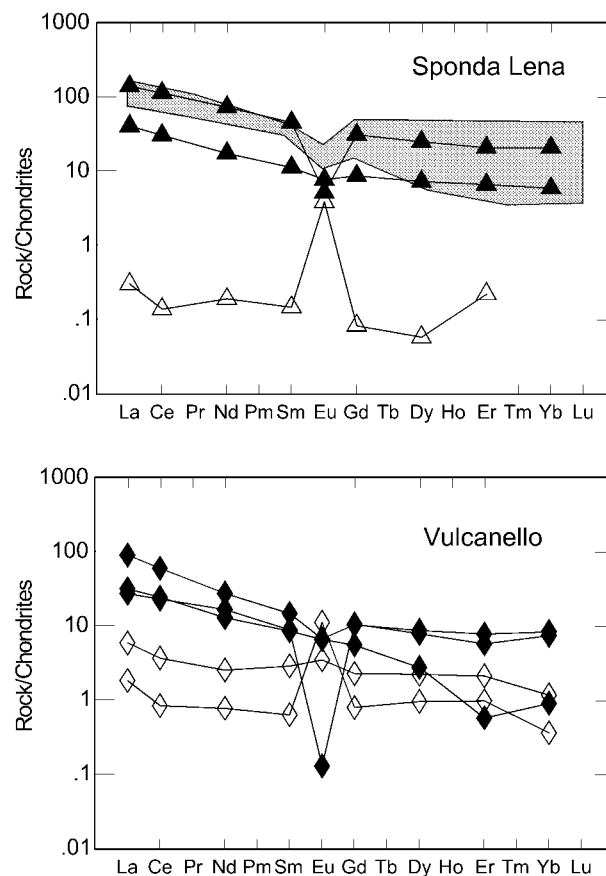
Fig. 7. Primordial mantle normalized incompatible element patterns for the analysed inclusions, for metamorphic rocks of the Calabro-Peloritano basement (grey shaded field). Symbols as in Fig. 6; filled and open symbols indicate early ITE-enriched and late ITE-depleted compositions, respectively.

Fig. 8. Chondrite-normalized REE patterns of the analysed melt inclusions compared with the metamorphic rocks of the Calabro-Peloritano basement (grey shaded field). Symbols as in Fig. 7.

3. the role of interaction between crustal- and mantle-derived melts in the Aeolian arc.

Nature of the quartz-rich xenoliths

Quartz-rich xenoliths are a common feature in lavas and pyroclastic deposits throughout the Aeolian arc. Previous studies of xenoliths from the island of Alicudi (Peccerillo & Wu, 1992; Peccerillo *et al.*, 1993) reported variable bulk-rock compositions for both major and trace elements, except for Rb, Cs and K, which were present at very low concentration levels. These data were used to suggest that the quartz-rich xenoliths represented refractory partial-melting residues of gneisses and other quartz-rich metamorphic rocks, which were incorporated in the magma and were strongly disaggregated during magma uprise. The variation in major and trace element contents suggested incremental melting of the protoliths, with different phases progressively entering the melt; biotite was consumed early, thus explaining the low concentration of Rb, Cs and K in all the xenoliths. Other

phases, such as accessory zircon, were inferred to enter the melt phase at a later stage, resulting in progressive depletion of Zr, REE and Th in the most refractory residues.

The two bulk-rock xenoliths analysed in this study show extreme enrichment in silica and low concentrations of other major and trace elements. Mantle-normalized incompatible element patterns are much more depleted than those of the analysed quartz-rich metamorphic rocks from the Calabro-Peloritano basement (Fig. 3). Moreover, silica-rich glass films are observed around the quartz grains (Fig. 2b), which record melting processes. All these features support the hypothesis that the analysed xenoliths represent residues left after partial melting of quartz-rich metamorphic rocks, which were more or less strongly disaggregated during transport to the surface by magma (see Honnorez & Keller, 1968; Peccerillo & Wu, 1992; Peccerillo *et al.*, 1993). The contrast between the abundance of quartz-rich xenoliths in the Aeolian magmas and the scarcity or absence of quartzites in the basement rocks cropping out in the Calabro-Peloritano

basement (Schenk, 1984) provides further evidence in favour of a restite hypothesis. Other restitic material, including cordierite, garnet and sillimanite, is found as xenolith-xenocrysts in the Aeolian arc lavas (e.g. Barker, 1987).

Genesis of silica-rich melt inclusions

The chemical analyses of the melt inclusions in the xenoliths indicate persilicic compositions, and important variation of other major and trace elements. The high-silica contents of all the inclusions, independent of the composition of the host volcanic material, preclude the possibility that they represent magmatic liquids entrapped in the quartz crystals and quenched during eruption at the surface. Therefore, we conclude that the melt inclusions represent silicic liquids formed by melting of basement metamorphic rocks and entrapped at different times within quartz grains. Understanding the geochemical composition and the variability of these inclusions may furnish important information on the processes that occurred during crustal anatexis. These melts, in fact, may provide evidence for different stages of anatexis and/or melt evolution, which are difficult to identify by studies of intrusive granites and related rocks.

One of the outstanding compositional features of the glasses in the studied inclusions is their very high silica content. This is unlikely to be an artefact caused by melting of the host quartz at the inclusion walls, during high-temperature experiments, contaminating the inclusions, as unheated melt inclusions have similar high-silica compositions (i.e. analyses performed before melting experiments, not reported). Nor do the high-silica contents result from chemical analysis contamination by host quartz caused by a large beam size, as SiO_2 amounts are unrelated to the size of inclusion. Neither is there evidence of loss of alkalis or other major and trace elements by diffusion into the host quartz, as several microprobe analyses on quartz surrounding the inclusions revealed no compositional change. Therefore, the compositions of the glasses are assumed to represent those of the entrapped melts.

Variation of major elements vs CaO (Fig. 6) reveals poorly defined negative trends for Al_2O_3, TiO_2, SiO_2 and K_2O, and rough positive trends for MgO, FeO and MnO (not shown). In general terms, this variability may be due to either fractional crystallization of the trapped anatectic melts or variable degrees of partial melting of the metamorphic protoliths. Although discriminating between these two processes is a difficult task, petrographic observations and the variation of major and trace elements do not fit fractionation processes.

As discussed above, the textures of the quartz grains in the xenoliths are diverse. Q_1 quartz grains are interpreted to represent residual phases. Their rounded or spongy morphology, coupled with the presence of intergranular glass (Fig. 2b–d), suggests a relation with melting processes, as also indicated by the abundant melt inclusions. The presence of a cristobalite rim around many Q_1 grains (Fig. 4a) further suggests that SiO_2 from the melt nucleated on the matrix quartz. Conversely, Q_2 polygonal grains are never associated with glass, neither in veins nor as inclusions. Q_2 grains may represent quartz crystals that were directly in contact and did not participate in the melting, but eventually recrystallized (annealing, Fig. 2e). An important implication of this conclusion is that various batches of melts produced at different stages of melting and extraction may have been trapped as inclusions within Q_1 quartz crystals, and that the melt inclusions may represent primary melt compositions.

From a petrological point of view, assuming that the most CaO-rich inclusions are parents to CaO-poor inclusions, mass balance calculations (e.g. Stormer & Nicholls, 1978) suggest that the average composition of the most CaO-poor melts can be broadly obtained from the least silica-rich inclusions after 30–40% fractional crystallization dominated by K-feldspar, plagioclase and some biotite. However, the calculated residual liquids do not match satisfactorily the observed compositions and the sum of residual oxides never drops below 5–6%. Trace element variations also indicate several difficulties with a fractional crystallization model. Compositions of ITE-enriched inclusions cannot be obtained by fractional crystallization starting from depleted inclusions. Such a process is unable to provide an increase for some elements (e.g. Zr, Y) that is greater than 2–3 orders of magnitude. On the contrary, the Zr and REE concentrations of the ITE-depleted inclusions can be obtained easily from ITE-enriched melts by fractional crystallization, assuming a compatible behaviour for these elements. This simply requires that accessory zircon and monazite or allanite were present as accessory fractionating phases. These minerals have very high partition coefficients for REE, and Zr (>1000, e.g. Sawka, 1988), and their presence in accessory amounts in the separating assemblage is able to decrease ITE concentrations dramatically. However, the Sr, Ba and Rb contents of ITE-depleted inclusions implies, in most cases, a compatible behaviour also for these elements, requiring feldspar and biotite fractionation. Rb is generally incompatible in the silica-rich melts, unless biotite participates very heavily during fractionation (some 50% of solid, assuming $K_{biotite/liquid} = 5$). Also, feldspar fractionation conflicts with the presence of strong positive Eu anomalies in the ITE-depleted inclusions.

Therefore, the compositional variability of melt inclusions does not appear to be generated by

fractionation processes, but probably reflects the primary compositions of the anatectic melts. Assuming that the analysed metamorphic rocks are parental to the melt inclusions, the high-silica contents of the glass inclusions testify to the substantial participation of quartz in the melting assemblage. The variable CaO content may reflect either variability in the metamorphic rocks, and/or variable degrees of partial melting; this is supported by the negative correlation between CaO and SiO_2 and the rough positive trends of CaO vs MgO and FeO_{total}. The higher K/Na and lower Al_2O_3 of the melt inclusions compared with the basement metamorphic rocks (Fig. 6) support a role for K-feldspar melting. The increase of K/Na with decreasing CaO may reveal an increasing role for K-feldspar with decreasing degree of partial melting. Similarly, the invariably high K_2O contents and the lack of correlation between K and Ba (which is hosted in K-feldspars) requires melting of K-rich phases other than K-feldspar, e.g. biotite. Biotite melts incongruently, according to the reaction

$$Biotite + Quartz + Plagioclase$$
$$= Orthopyroxene \pm Oxides + melt$$
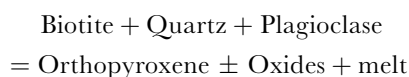
giving melts with high K/Fe; this explains the vertical trend of K_2O/FeO ratio in the most CaO-poor compositions (Fig. 6), revealing early entry of biotite into the melt. Incongruent melting of biotite in the early stages of partial melting is consistent with the high ASI numbers of the melt inclusions, with the absence of H_2O in associated fluid inclusions, and with the estimated middle- to lower-crustal conditions for partial melting processes, i.e. high-grade metamorphic conditions where biotite is a stable phase. In this respect, the small grains of oxides and orthopyroxene rarely observed within some individual melt inclusions may represent a product of biotite breakdown reactions trapped along with the resultant anatectic melts. Muscovite is most likely to have been present, but appears to participate in melting only in the initial stages (Patiño-Douce & Johnston, 1991; Patiño-Douce & Harris, 1998). There is no evidence for the presence of sillimanite as a residual phase in either the melt inclusions or the host xenoliths. It should be noted, however, that sillimanite has been commonly found in other crustal xenoliths from nearby Lipari Island (Honnorez & Keller, 1968; Pichler, 1980; Barker, 1987).

The CIPW normative compositions of the glass inclusions are plotted on a Qz–Ab–Or ternary plot (Fig. 9) (Ebadi & Johannes, 1991). Among the early-trapped melts, only a few have near minimum melt major-element compositions and plot close to the haplogranite eutectic points for low pressures (i.e. ≤1 kbar). However, low-pressure conditions do not correspond to
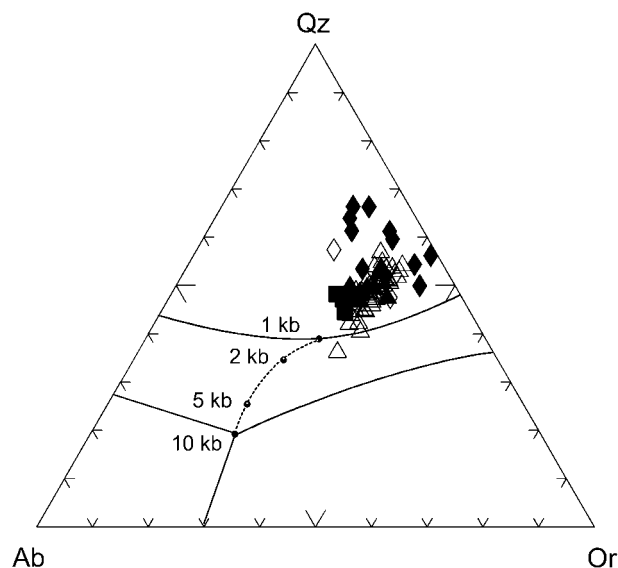
Fig. 9. CIPW normative compositions of the glass inclusions plotted on a Qz–Ab–Or diagram (Ebadi & Johannes, 1991). Symbols as in Fig. 7.

trapping pressures calculated from a recent fluid inclusion study, which indicated that the high-silica melts formed at pressures between 3·5 and 5·6 kbar (Zanon et al., 2003). This is only an apparent contradiction, however, as it might simply indicate that temperatures were higher than the eutectic during partial melting. Such a hypothesis is substantiated by melt-inclusion microthermometry, indicating that temperatures exceeded 900°C during melting of the parental metamorphic rocks. Experimental studies have shown that in the lower crust, in situ dehydration melting of fertile pelitic lithologies at temperatures in excess of 800°C may generate substantial amounts of water-undersaturated, peraluminous, rhyolitic melt of near-minimum composition (Clemens, 1990; Patiño-Douce & Johnston, 1991).

The distribution of the glass compositions reveals an apparent trend of decreasing normative Ab from early to late-trapped melts, together with a linear increase of the Qz/Or ratio (Fig. 9). These compositional trends could be the result of several processes, among which are different proportions of the various mineral phases involved in the partial melting process, or a rapid extraction of the melts produced. On the assumption that all the Na_2O derives from melting of plagioclase, the observed correlation suggests that plagioclase was progressively consumed during partial melting.

Modelling crustal melting: trace element patterns in enriched and depleted inclusions

Analysis of the trace element data allows a deeper insight to be gained into the processes of crustal
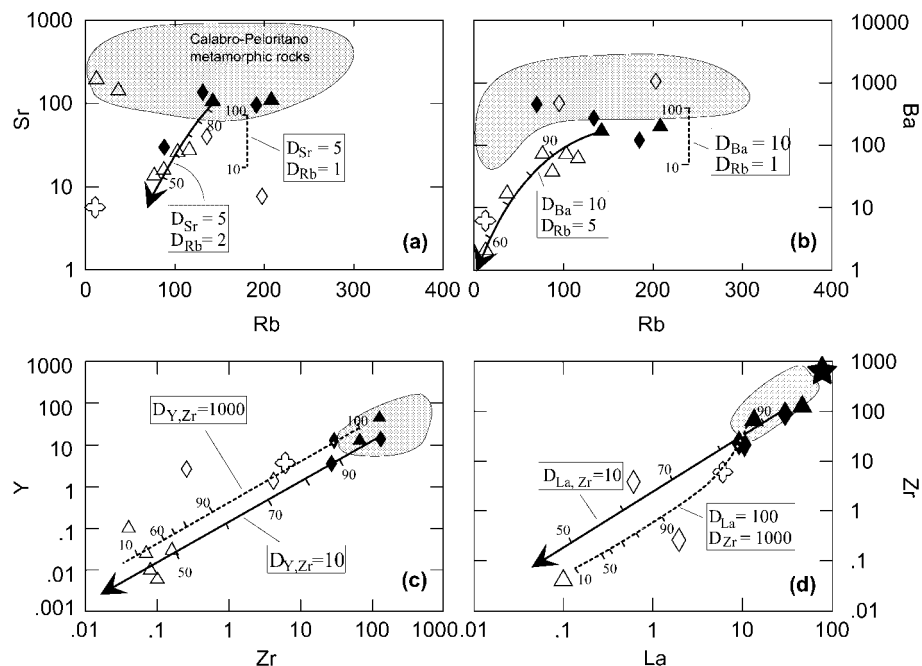
Fig. 10. Element–element variation diagrams (log–log scale) for the analysed inclusions and for the metamorphic rocks of the Calabro-Peloritano basement (grey fields). Continuous lines represent fractional crystallization models starting from ITE-enriched inclusions toward ITE-depleted inclusions. Dashed lines are fractional melting models. Partition coefficients used have been arbitrarily chosen to satisfactorily fit the fractional crystallization and melting processes (for further explanation, see text). Batch melting gives similar results to fractional melting. In the Zr vs La diagram (d), the star represents the equilibrium composition of a peraluminous acid melt saturated with zircon and REE-monazite, calculated according to Watson & Harrison (1983) and Montel (1993). Numbers along the model curves indicate the amount of melt. The open cross indicates the composition of the quartz xenoliths; other symbols as in Fig. 7.

anatexis. The analysed inclusions show large variations in ITE abundances, particularly for REE, Y, Nb and Zr, which vary over three orders of magnitude at Sponda Lena and more than one order of magnitude at Vulcanello. On the other hand, Rb and Cs vary less, and generally fall within the compositional range of Calabro-Peloritano metamorphic rocks. As the trace element content of quartz is negligible, the observed large chemical variations are unlikely to result from different quartz–melt partition coefficients and/or from the rate of diffusive transport in the glass contained in the melt inclusions relative to the host mineral. Observed differences are, therefore, melt-related features and must be related to source compositions and processes involved in the melt generation.

Modelling of partial melting processes to generate the analysed inclusions presents several difficulties. These arise, among others, from the lack of knowledge of the precise nature and composition of the source metamorphic rocks, and of the physical process of melt formation and extraction, and from the difficulty in calculating reliable partition coefficients for the residual phases. In the following discussion, we use the analysed metamorphic rocks as source rock compositions. Moreover, models are calculated by assuming

that trace elements can be hosted both in the major phases (notably, hornblende, e.g. Pearce & Norry, 1979) and in the accessory phases; in the first case, trace element behaviour during anatexis is modelled by using classical fractional melting equations (e.g. O'Hara *et al.*, 2002, and references therein); in the latter case, ITE are major components of accessory phases and do not obey Henry's law (Watson, 1985), and anatectic melt compositions are calculated using the equations suggested by Watson & Harrison (1983) and Montel (1993). Difficulties in establishing reliable partition coefficients ($D_{s/l}$) for use in modelling fractional melting processes are overcome by following a reverse approach: we choose the best values of $D_{s/l}$ to fit the trace element variations in the analysed inclusions, and successively explore the implications of these best-fit values.

A fractional melting model for the analysed metamorphic rocks and inclusions is indicated by dashed lines in Fig. 10. The compositions of late ITE-enriched inclusions (filled symbols) fall in the field of the Calabro-Peloritano basement (shaded) for most of the trace elements. Therefore, their trace element composition can be easily explained by assuming high degrees (>80%) of partial melting of the metamorphic rocks.

The similar REE patterns of the inclusions and the metamorphic rocks also support this hypothesis (see Fig. 7).

In contrast, the early ITE-depleted inclusions show abundances and patterns of several trace elements that are difficult to explain by fractional melting of the analysed metamorphic rocks. Rb concentrations fall in the range of the basement metamorphic rocks (Fig. 10b), and can be modelled either by large degrees of melting of metamorphic rocks, or by moderate to low degrees of melting with partition coefficients between melt and residue around unity. These conditions require biotite as a residual phase. The Ba and Sr contents of the inclusions show a wide range of values, with some inclusions falling in the field of metamorphic rocks, but others displaying lower concentrations. Fractional melting of metamorphic rocks reported in Fig. 10a and b shows that the Sr–Ba-depleted compositions can be explained only by assuming high partition coefficients for these elements. For example, the low Ba concentrations of some of the inclusions can be reached only if $D_{Ba} > 10$; also the low Sr of a few inclusions requires $D_{Sr} > 10$. These partition coefficients are unlikely, as they cannot be attained even in the case that the residue was formed of pure feldspars.

Other trace elements (e.g. LREE, Zr and Y) also create some problems. If the ITE-enriched inclusions fall inside or close to the field of metamorphic rocks, supporting a derivation by high degrees of partial melting (Fig. 10c and d), the ITE-depleted inclusions display much lower concentration than the metamorphic rocks. These values can be obtained only by assuming a compatible behaviour for these elements. Fractional melting models of metamorphic rocks require partition coefficients as high as 100–1000, to account for the low Y, La and Zr. This is possible only if accessory Zr- and REE-rich phases, such as zircon and monazite, are present in the residue, as generally accepted for silicic crustal systems (e.g. Ayres & Harris, 1997). Harrison & Watson (1983), Watson & Harrison (1983) and Montel (1986, 1993) showed that the equilibrium partition coefficients of Zr and REE between zircon, monazite and melt are a function of various parameters, including magma composition, water concentration, accessory mineral composition and temperature. Temperature has important effects on accessory mineral solubility. Experimental evidence has demonstrated that Zr and La concentrations in peraluminous liquids in equilibrium with zircon and REE-monazite show concentrations of tens to hundreds of ppm at the onset temperatures of crustal anatexis (i.e. 650–700°C). At temperatures of 1000–1100°C (i.e. trapping temperature of the analysed inclusions), REE and Zr reach concentrations of several hundred to a thousand ppm, respectively

(Watson & Harrison, 1983; Montel, 1993). These concentrations drop to slightly lower values in the case of natural zircon and allanite as a result of the decrease of Zr and REE activity; however, concentrations still remain higher by 2–3 orders of magnitude compared with those observed in the ITE-depleted melt inclusions (Fig. 10c and d). Values of Zr and La calculated for peraluminous melts containing 4% H_2O in equilibrium with zircon and REE-monazite at 1000°C (black star) are reported in Fig. 10d.

An alternative explanation is that the depleted inclusions do not derive from melting of fertile metamorphic rocks, but from previously depleted restites, which have lost their ITE during an earlier stage of melting. Such a two-stage model requires that trace elements are incompatible during the first-stage melting (i.e. went into the liquid), whereas they are compatible during the second stage (i.e. were left in the residue). Such a hypothesis is, however, in contradiction to the petrographic and $P-T$ studies, which clearly indicate that: (1) both enriched and depleted inclusions formed at the same P and T conditions during a single melting event; (2) depleted inclusions were formed at an earlier stage of melting than enriched inclusions. Moreover, it would be difficult to envisage that a residual melt with low ITE contents could contain accessory phases to be left in the residue during the second-stage partial melting.

Trace element and REE patterns similar to those of the early ITE-depleted inclusions (i.e. depletion in REE except for Eu, resulting in strong Eu positive anomalies) are commonly observed in anatectic leucosomes present in granulite-facies migmatites (e.g. Ayres & Harris, 1997; Jung et al., 2000). In leucosomes, low abundances of REE have been attributed to the failure of accessory phases (e.g. zircon, apatite, monazite) to equilibrate with the melt (e.g. Sawyer, 1991; Watt & Harley, 1993; Carrington & Watt, 1995).

Low trace element contents can occur because of several factors, including: (1) low diffusion of elements with respect to the rate of melt formation and extraction (i.e. not enough time to attain equilibrium conditions: disequilibrium melting); (2) melts do not come into physical contact with accessory minerals, thus preventing solid–liquid diffusion of ITE (i.e. not enough elements available to enter the liquid)—such a condition is very likely whenever the degrees of partial melting are low, and accessory minerals are shielded in intergranular positions among the major phases; (3) low water contents in melts result in long dissolution times for accessory phases and equilibrium may not be attained (i.e. not enough time). These three possibilities are not exclusive, and all are able to cause the ITE contents of liquids coexisting with accessory phases to be less enriched then expected.

It has been long established (Smith *et al.*, 1955) that equilibrium conditions during partial melting are attained only when the formation of melt and its successive extraction occurs over time spans that are long enough to allow smoothing of chemical potentials in the system. The length of time necessary for equilibrium to be reached is a function of the mobility of the different elements both in the solid phases and in the coexisting liquid. Experimental data and theoretical modelling of element mobility in silicate melts have demonstrated that diffusivities depend both on the intrinsic characteristics of the elements (i.e. ionic radius, charge) and on the physical properties of the system (structure and viscosity of silicate melts; e.g. H_2O content) (Hoffman, 1980; Kushiro, 1980; Chakraborty, 1995; Perez & Dunn, 1996; Liang *et al.*, 1997). Despite the complexity of the problem, data and modelling agree in indicating that in highly polymerized melts (e.g. haplogranite) the high field strength elements [HFSE; i.e. those elements with squared charge over ionic radius $(z_2/r) > 10$; e.g. Zr, Nb, Th] have much lower diffusion coefficients than intermediate field strength element (IFSE; i.e. those with $1 < z_2/r < 10$, e.g. Ba, Sr) and alkalis (e.g. Nakamura & Kushiro, 1998; Mungall, 2002). In addition, Mungall (2002) showed that, unlike HFSE and IFSE, diffusivity of alkalis is basically independent of the melt viscosity and, as a consequence, is high even in strongly polymerized melts. This implies that high-silica melts formed by crustal anatexis may have near-equilibrium compositions for alkalis, but not for HFSE and, to a lesser degree, IFSE.

As far as REEs are concerned, high-pressure experimental data for highly polymerized melts, reported by Nakamura & Kushiro (1998), have shown that there is a decrease of diffusivity with increasing ionic radius. However, Eu displays an anomalous and much higher diffusion coefficient than the other REE, and can be enriched with respect to other REE in crustal anatectic melts. This may be an explanation of the positive Eu spikes commonly encountered in crustal anatectic rocks, as well as in some of the analysed melt inclusions. Low diffusivities of several trace elements, especially HFSE, in highly polymerized melts make disequilibrium melting the most probable cause for low HFSE contents in melt formed during crustal anatexis (Sawyer, 1991; Watt & Harley, 1993; Carrington & Watt, 1995). On the other hand, the variable diffusivities of different ions are expected to produce variable departures from equilibrium conditions for the different elements, with progressively greater depletions passing from alkalis to IFSE and HFSE.

The early, ITE-depleted inclusions in this study have similar major element compositions to the late, enriched ones, with high Na_2O and K_2O, and Rb and Cs contents that are similar to the (parent) metamorphic rock compositions. On the contrary, Sr and Ba have variable concentrations, some of which are exceedingly low and difficult to explain by equilibrium melting. HFSE and REE contents are also very low, with the exception of Eu, which shows a pronounced positive anomaly with values close to concentrations observed in the metamorphic rocks. All these data fit well the hypothesis that the analysed depleted inclusions could be derived by disequilibrium melting of metamorphic rocks, and the concentrations of the various elements reflect variable diffusivities in silica-rich melt systems.

In our opinion, however, the concentrations of HFSE (e.g. Y and Zr) are exceedingly low in some inclusions from Sponda Lena (Table 3). Leucosomes formed by disequilibrium melting in high-grade metamorphic terranes generally have abundances of Zr of the order of 10 ppm or of several tens of ppm (Ayres & Harris, 1997; Jung *et al.*, 2000). In addition, Zr is a major component of zircon, one of the most common accessory phases in the Calabro-Peloritano metamorphic rocks. Theoretical models also suggest that high Zr contents are to be expected in melts formed at 1000°C from a fertile metamorphic rock containing this phase.

It is therefore proposed that the extreme depletion in some ITE should be attributed to the insufficient amount of these elements to saturate the melt, as a result of shielding of accessory phases by the main mineral phases during melting processes. According to this hypothesis, whereas the variable concentrations of elements that are hosted in the main phases (i.e. alkalis, Ba, Sr and Eu) reflect variable diffusivities, the contents of some HFSE may depend on both the low element diffusivities and the small degrees of partial melting, which generated isolated melt drops and did not allow these drops to come into contact with accessory phases.

In conclusion, the studied melt inclusions record distinct stages during a single crustal melting process, which produced high-silica rhyolitic melts displaying a sharp increase of ITE from early- to late-produced melts. During the early stages of melting, formation of high-silica melts occurs through the breakdown of quartz, feldspars ± biotite, whereas the accessory phases remain in the residue (Fig. 11a). Melting begins at grain edges and corners where the reactant minerals are in contact, and because of the small melt fractions, the accessory phases do not even come into contact with melts produced. Consequently, early anatectic melts form small grain-scale films and pools that remain isolated along grain boundaries and become trapped as inclusions (Fig. 11a and b). Such a possibility is very likely, given the high viscosity of silica-rich melts, which requires high degrees of partial melting for the liquid drops to coalesce and form a continuous

Crustal melting
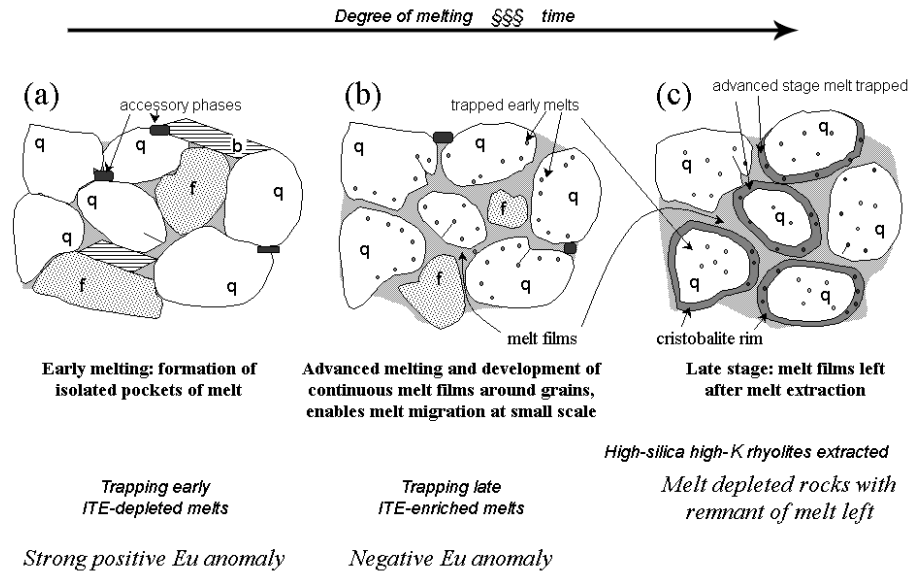
Fig. 11. Schematic model for the formation of anatectic crustal melts as recorded by melt inclusions trapped in quartz xenoliths from Vulcano Island. During the early stages, high-silica melts formed *in situ* through breakdown of quartz, feldspars ± biotite (a); because of the very small melt fractions, most of the accessory minerals did not come into contact with the melt. Early anatectic melts formed small pools or pockets that remained isolated along grain boundaries and grain corners and were later trapped as inclusions. This and the low ITE diffusivities generated depletion in HFSE and in REE, and a strong positive Eu anomaly in the melt. At higher degrees of partial melting, melts were formed with both major and accessory phases entering the melt, generating liquids with trace element contents comparable with those of the metamorphic source rocks (b). The higher abundance of melt also allowed formation of an interconnecting melt film, the formation of which allowed melt migration and silica crystallization (cristobalite rim). Separation of the melt from the residue initiated the formation of the high-K, high-Si magma (c). q, quartz; f, feldspar; b, biotite.

network (Sawyer, 2001). This and the low ITE diffusivities have produced the depletion for HFSE and for REE, and the strong positive Eu anomaly in the melts. It is noteworthy that this process should not be confused with disequilibrium melting, as this latter process depends only on time. In our case even if time were infinite, the melt still would not be saturated in ITE (insufficient elements to saturate the melt).

At higher degrees of partial melting, melts are formed with both major and accessory phases participating in the melting (Fig. 11b). High degrees of melting (<80%) generate late liquids with trace element contents comparable with those of the metamorphic source rocks (Figs 7 and 10). The higher abundance of melt also allows the formation of a more extensive branching network, which initiates melt migration and favours draining of the melt from the solid residue. The formation of a linked network of melt films enclosing residual minerals induces new crystal growth, represented by the cristobalite overgrowth observed on many residual quartz grains. At this stage, ITE-enriched melt inclusions are trapped within residual quartz and new cristobalite growth (Fig. 11c).

The trace element depleted quartz-rich xenoliths analysed at Vulcano represent the residue left after extraction of these late and more enriched anatectic melts (Fig. 11c).

Implications for interaction between crustal- and mantle-derived melts in the Aeolian arc

A substantial number of studies have shown that magmas in the Aeolian arc have undergone strong interaction with crustal materials [see De Astis *et al.* (2000) for summary and discussion]. The occurrence of quartz-rich, restitic crustal xenoliths in lavas and pyroclastic rocks represents the most outstanding evidence for this process. However, there is debate about the relative roles of crustal assimilation vs compositional anomalies in the mantle in determining the geochemical and isotopic characteristics of rocks at Vulcano and other Aeolian islands. According to some workers (e.g. Esperanca *et al.*, 1992), the transition from calc-alkaline to potassium-rich magmatism could result from interaction between mantle-derived calc-alkaline melts and the continental crust; other workers, although recognizing an important role for assimilation processes, have suggested that the mafic rocks, each with a different level of enrichment in

potassium, represent distinct magma types generated from heterogeneous mantle sources (e.g. Ellam *et al.*, 1988, 1989; Ellam & Harmon, 1990; De Astis *et al.*, 2000).

Mafic shoshonitic and K-alkaline rocks from younger eruptions at Vulcano have higher enrichments in incompatible elements than do older HKCA mafic rocks (e.g. De Astis *et al.*, 2000). Ratios of incompatible trace elements are also variable, and this eliminates the possibility that the various mafic magmas are related to each other by fractional crystallization or by different degrees of partial melting of a homogeneous mantle source. Variation in radiogenic isotope ratios at Vulcano led De Astis *et al.* (1997) to infer strong interaction between the early HKCA magmas and crustal material of the Calabro-Peloritano basement. However, this process was unable to explain the transition from calc-alkaline to potassic magmatism (De Astis *et al.*, 2000).

Geochemical data that have been traditionally used to model magma–crust interaction in the Aeolian arc come from metamorphic xenoliths entrained in volcanic rocks and the whole-rock compositions of key lithologies from the Calabro-Peloritano basement (Ellam & Harmon, 1990). The approach of Ellam & Harmon (1990), however, has a number of limitations, as it assumes bulk assimilation of basement metamorphic rocks. A much more realistic contaminant for mantle-derived mafic magmas may be partial melts derived from the basement metamorphic rocks. Previous discussion has shown that glass inclusions in quartz crystals represent melts formed by anatexis of metamorphic rocks. Therefore, the melt inclusions may represent a more realistic composition for the contamination of the Aeolian magmas. Here, we use the new data from the melt inclusions to test whether models based on bulk metamorphic rock assimilation or on mixing between Aeolian magmas and anatectic crustal melts provide the best fit to the compositional characteristics of the volcanic rocks.

Trace element variations in the Vulcano rocks and the analysed melt inclusions are plotted in Fig. 12. Simple mixing models (dashed line) show that it is possible to explain the potassium and Rb contents of shoshonites and KS (Younger Vulcano rocks; grey field in Fig. 12) by mixing between anatectic melts similar to those preserved in the inclusions and mafic HKCA magmas (Older Vulcano rocks; open field in Fig. 12). However, most incompatible trace elements (e.g. REE, Nb, Zr) are lower in the inclusions than in the younger Vulcano rocks, and mixing with HKCA magma cannot generate the observed ITE enrichments. On the other hand, if contemporaneous fractionation is assumed during mixing, ITE enrichment is obtained; but this also generates a strong decrease in compatible

elements, which is not observed in the mafic shoshonites and KS (De Astis *et al.*, 2000).

In conclusion, the newly obtained data on melt inclusions provide further support to the hypothesis that simple processes of magma–crust interaction (i.e. bulk assimilation and/or mixing with crustal anatectic melts) are unable to produce the transition from calc-alkaline to shoshonitic and potassic magmatism. However, we cannot exclude the possibility that the composition of the anatectic melts might be more variable than those inferred on the basis of the melt inclusion study reported here. Additional studies on glass inclusions in metamorphic xenoliths may be important for providing further data on crustal anatectic melt compositions and to constrain the effects that mixing of these melts can have on mantle-derived magmas.

CONCLUSIONS

Melt inclusions present in quartz-rich xenoliths in lavas at Vulcano represent melts formed by the anatexis of crustal rocks beneath the Aeolian arc. Major elements in homogenized inclusion glasses show a wide range of concentrations, but all display high enrichment in silica and potassium and resemble high-K rhyolites. Rb and Cs contents are generally high and similar in concentration to those in metamorphic rocks from the Calabro-Peloritano basement. Other trace element abundances are more variable, with concentrations of some elements such as Nb, Zr and REE spanning more than three orders of magnitude. Some inclusions have relatively high incompatible trace elements concentrations, close to those of the Calabro-Peloritano metamorphic rocks. Others are exceedingly depleted in ITE, with Zr, Y and REE ranging from a few ppm to fractions of a ppm. Textural evidence suggests that the depleted inclusions were trapped earlier than the enriched ones, during the same melting event.

Geochemical modelling suggests that the ITE-enriched inclusions have been formed by large degrees of batch melting of gneiss and schists, leaving a quartz-rich residue. The quartz-rich xenoliths that host the studied melt inclusions are ubiquitous in the Aeolian volcanic rocks, and most probably represent the restitic material left after formation and extraction of ITE-enriched melts. The compositions of the ITE-depleted inclusions cannot be generated by fractional melting of any fertile metamorphic rocks, and geochemical modelling suggests that silica-rich melts did not reach chemical equilibrium with the residual phases. Departure of element abundances from equilibrium concentrations are greater for HFSE than for IFSE and alkalis. This may reflect variable diffusivities of the elements or/and the lack of physical contact between small melt fractions and residual accessory phases, which host HFSE.
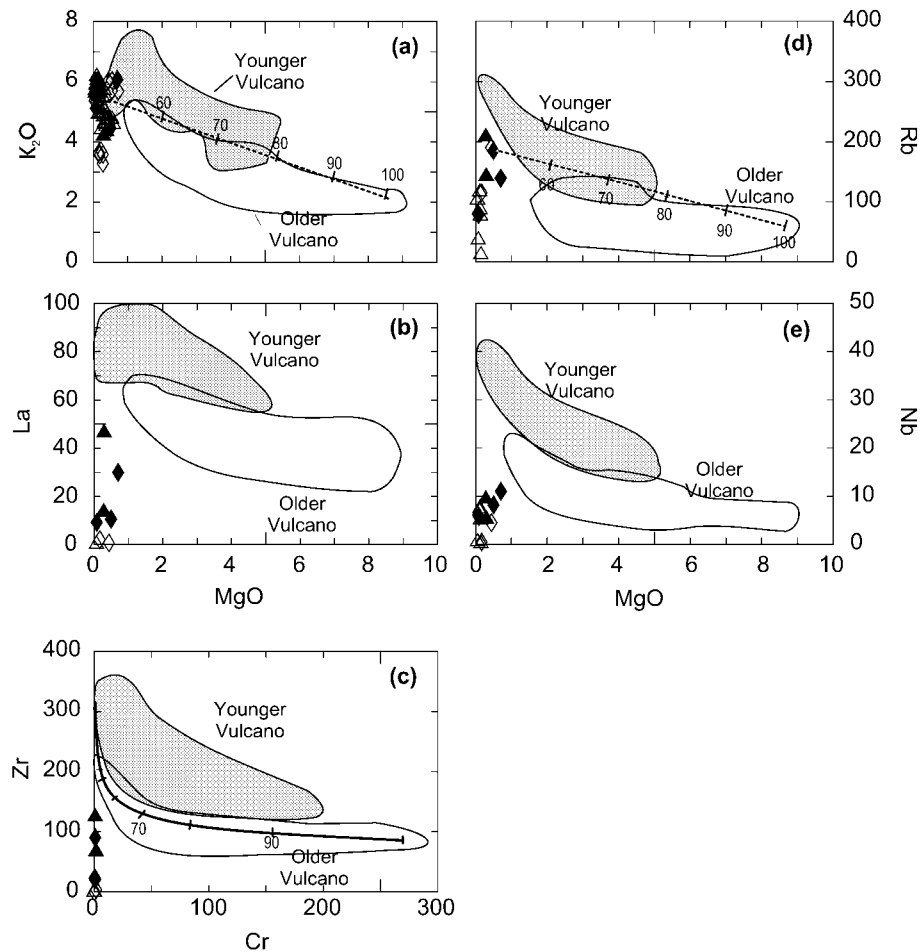
Fig. 12. Trace element variation for the Vulcano rocks and for the analysed melt inclusions. Two end-member mixing (a and d): average older Vulcano basalts (De Astis *et al.*, 2000) and melt inclusion data are indicated. The model curve on the Cr vs Zr diagram (c) is a mixing plus fractional crystallization model from a mafic HKCA magma, assuming compatible behaviour for Cr ($D = 5$) and incompatible behaviour for Zr ($D = 0.1$), starting from older Vulcano basalts (De Astis *et al.*, 2000) and assuming average Calabro-Peloritano crustal rocks (Rottura *et al.*, 1991) as contaminant. The ratio between assimilated and crystallized mass is set at 0.2. Symbols as in Fig. 7. Older Vulcano and Younger Vulcano data are from De Astis *et al.* (2000).

Melt inclusions represent snapshots of the liquids at a specific stage of crustal melting, and preserve the chemical characteristics of the liquids formed at the various stages of melting. Therefore, the data provide important information on mechanisms of crustal melting.

Melt inclusions also represent the remains of possible contaminants of the mantle-derived magmas and they have been used to test the effects of interaction between mantle-derived magma and crustal material in the Aeolian arc, especially the possibility that shoshonitic and potassic alkaline magmas originated from parental calc-alkaline melts. Most of the analysed inclusions have high potassium concentrations and mixing with calc-alkaline magmas may drive their composition towards shoshonitic and potassic alkaline suites. However, the melt inclusions have ITE concentrations comparable with those of the calc-alkaline magmas and lower abundances than either the shoshonites or K-alkaline rocks. Therefore, they are unable to provide the budget of incompatible trace elements that is necessary to reach potassic compositions.

REFERENCES

Albarède, F. (1992). How deep do common basaltic magmas form and differentiate? *Journal of Geophysical Research* **97**(B7), 10997–11009.

Ayres, M. & Harris, N. (1997). REE fractionation and Nd-isotope disequilibrium during crustal anatexis: constraints from Himalayan leucogranites. *Chemical Geology* **139**, 249–269.

Barker, D. S. (1987). Rhyolites contaminated with metapelite and gabbro, Lipari, Aeolian Islands, Italy: products of lower crustal fusion or of assimilation plus fractional crystallization? *Contributions to Mineralogy and Petrology* **97**, 460–472.

Bonardi, G., D'Argenio, B. & Perrone, V. (1988). Carta Geologica dell'Appennino Meridionale. *Memorie della Società Geologica Italiana* **41**, 1341, Tav. 1.

Carrington, D. P. & Watt, G. R. (1995). A geochemical and experimental study of the role of K-feldspar during water-undersaturated melting of metapelites. *Chemical Geology* **122**(1–4), 59–76.

Castellet y Ballarà, G., Crescenzi, R., Pompili, A. & Trigila, R. (1982). A petrological model on magma evolution of Vulcano eruptive complex (Aeolian Islands—Italy). In: Coradini, A. & Fulchignoni, M. (eds) *The Comparative Study of Planets. NATO Advanced Study Institutes Series, D.* Dordrecht: Reidel, pp. 459–476.

Chakraborty, S. (1995). Diffusion in silicate melts. In: Stebbin, J. F. (ed.) *Structure, Dynamics and Properties of Silicate Melts. Mineralogical Society of America, Reviews in Mineralogy* **32**, 411–503.

Clemens, J. D. (1990). The granulite–granite connexion. In: Vielzeuf, D. & Vidal, P. H. (eds) *Granulites and Crustal Evolution.* Dordrecht: Kluwer, pp. 25–36.

Clocchiatti, R., Del Moro, A., Gioncada, A., Joron, J. L., Mosbah, M., Pinarelli, L. & Sbrana, A. (1994). Assessment of a shallow magmatic system: the 1888–90 eruption, Vulcano Island, Italy. *Bulletin of Volcanology* **56**, 466–486.

Czamanske, G. K., Sisson, T. W., Campbell, J. L. & Teesdale, W. J. (1993). Micropixe analyses of silicate reference standards. *American Mineralogist* **78**(9–10), 893–903.

De Astis, G., La Volpe, L., Peccerillo, A. & Civetta, L. (1997). Volcanological and petrological evolution of Vulcano island (Aeolian Arc, southern Tyrrhenian Sea). *Journal of Geophysical Research* **102**(B4), 8021–8050.

De Astis, G., Peccerillo, A., Kempton, P. D., La Volpe, L. & Wu, T. W. (2000). Calcalkaline to potassium-rich magmatism in the Aeolian Arc: geochemical and Sr, Nd, Pb isotopic constraints from the Island of Vulcano (Aeolian arc). *Contributions to Mineralogy and Petrology* **139**, 684–703.

De Paolo, D. J. (1981). Trace elements and isotopic effects of combined wallrock assimilation and fractional crystallization. *Earth and Planetary Science Letters* **53**, 189–202.

Ebadi, A. & Johannes, W. (1991). Beginning of melting and composition of first melts in the system Qz–Ab–Or–H_2O–CO_2. *Contributions to Mineralogy and Petrology* **106**, 286–295.

Ellam, R. M. & Harmon, R. S. (1990). Oxygen isotope constraints on the crustal contribution to the subduction-related magmatism of the Aeolian Islands, Southern Italy. *Journal of Volcanology and Geothermal Research* **44**, 105–122.

Ellam, R. M., Menzies, M. A., Hawkesworth, C. J., Leeman, W. P., Rosi, M. & Serri, G. (1988). The transition from calc-alkaline to potassic orogenic magmatism in the Aeolian Islands, Southern Italy. *Bulletin of Volcanology* **50**, 386–398.

Ellam, R. M., Hawkesworth, C. J., Menzies, M. A. & Rogers, N. W. (1989). The volcanism of Southern Italy: role of subduction and the relationship between potassic and sodic alkaline magmatism. *Journal of Geophysical Research* **94**(B4), 4589–4601.

Esperança, S., Crisci, G. M., De Rosa, R. & Mazzuoli, R. (1992). The role of the crust in the magmatic evolution of the Island of Lipari (Aeolian Islands, Italy). *Contributions to Mineralogy and Petrology* **112**, 450–462.

Faccenna, C., Mattei, M., Funiciello, R. & Jolivet, L. (1997). Styles of back extension in the Central Mediterranean. *Terra Nova* **9**, 126–130.

Falsaperla, S., Lanzafame, G., Longo, V. & Spampinato, S. (1999). Regional stress field in the area of Stromboli (Italy): insight into structural data and crustal tectonic earthquake. *Journal of Volcanology and Geothermal Research* **88**, 147–166.

Franzini, M. & Leoni, M. (1972). A full matrix correction in X-ray fluorescence analysis of rock samples. *Atti Società Toscana di Scienze Naturali* **73**, 7–22.

Frezzotti, M. L. (2001a). Applicazione della microspettroscopia Raman agli studi di mineralogia e petrologia. *Plinius* **26**, 62–73.

Frezzotti, M. L. (2001b). Silicate-melt inclusions in magmatic rocks: applications to petrology. *Lithos* **55**, 273–299.

Harrison, T. M. & Watson, E. B. (1983). Kinetics of zircon dissolution and zirconium diffusion in granitic melts of variable water contents. *Contributions to Mineralogy and Petrology* **84**, 66–72.

Hildreth, W. C. & Moorbath, S. (1988). Crustal contribution to arc magmatism in the Andes of Central Chile. *Contributions to Mineralogy and Petrology* **98**, 455–489.

Hoffman, A. W. (1980). Diffusion in natural silicate melts: a critical review. In: Hargraves, R. B. (ed.) *Physics of Magmatic Processes.* Princeton, NJ: Princeton University Press, pp. 385–418.

Honnorez, J. & Keller, J. (1968). Xenolithe in vulkanischen Gesteiner der Äolischen Inseln (Sizilien). *Geologische Rundschau* **57**(3), 719–736.

Jung, S., Hoernes, S. & Metzger, K. (2000). Geochronology and petrology of migmatites from the Proterozoic Damara belt—importance of episode fluid present disequilibrium melting and consequences for granite petrology. *Lithos* **51**, 153–179.

Keller, J. (1980). The island of Vulcano. *Rendiconti Società Italiana di Mineralogia e Petrologia* **36**(1), 369–414.

Kushiro, I. (1980). Viscosity, density and structure of melts at high pressures and their petrologic applications. In: Hargraves, R. B. (ed.) *Physics of Magmatic Processes.* Princeton, NJ: Princeton University Press, pp. 93–120.

Liang, Y., Richter, F. M. & Chamberlin, L. (1997). Diffusion in silicate melts: III. Empirical models for multicomponent diffusion. *Geochimica et Cosmochimica Acta* **61**, 5295–5312.

Mason, B. & Allen, R. O. (1973). Minor and trace elements in augite, hornblende and pyrope megacrysts from Kakanui, New Zealand. *New Zealand Journal of Geology and Geophysics* **16**, 935–947.

25

Montel, J.-M. (1986). Experimental determination of the solubility of Ce-monazite in SiO_2–Al_2O_3–K_2O–Na_2O melts at 800°C and 2 kbar, under H_2O saturated conditions. *Geology* **14**, 659–662.

Montel, J.-M. (1993). A model for monazite/melt equilibrium and applications to the generation of granitic magmas. *Chemical Geology* **110**, 127–146.

Mungall, J. E. (2002). Empirical models relating viscosity and trace diffusion in magmatic silicate melts. *Geochimica et Cosmochimica Acta* **66**, 125–143.

Nakamura, E. & Kushiro, I. (1998). Trace element diffusion in jadeite and diopside melts at high pressures and its geochemical implication. *Geochimica et Cosmochimica Acta* **62**, 3153–3160.

O'Hara, M. J., Fry, N. & Prichard, H. M. (2002). Minor phases as carriers of trace elements in non-modal crystal–liquid separation processes. I: Basic relationships. *Journal of Petrology* **42**, 1869–1885.

Patino, L. C., Carr, M. J. & Feigenson, M. D. (2000). Local and regional variations in Central American arc lavas controlled by variations in subducted sediment input. *Contributions to Mineralogy and Petrology* **138**, 265–283.

Patiño-Douce, A. E. & Harris, N. (1998). Experimental constraints on Himalayan anatexis. *Journal of Petrology* **39**(4), 689–710.

Patiño-Douce, A. E. & Johnston, A. D. (1991). Phase equilibria and melt productivity in the pelitic system: implications for the origin of peraluminous granitoids and aluminous granulites. *Contributions to Mineralogy and Petrology* **107**, 202–218.

Pearce, J. A. & Norry, M. J. (1979). Petrogenetic implications of Ti, Zr, Y and Nb variation in volcanic rocks. *Contributions to Mineralogy and Petrology* **69**, 33–47.

Pearce, J. A., Perkins, W. T., Westgate, J. A., Gorton, M. P., Jackson, S. E., Neal, C. R. & Chenery, S. P. (1997). A compilation of new and published major and trace elements data for NIST SRM 610 and NIST SRM 612 glass reference materials. *Geostandards Newsletter* **21**, 115–144.

Peccerillo, A. & Taylor, S. R. (1976). Geochemistry of Eocene calc-alkaline volcanic rocks from Kastamonu area, Northern Turkey. *Contributions to Mineralogy and Petrology* **56**, 221–246.

Peccerillo, A. & Wu, T. W. (1992). Evolution of calc-alkaline magmas in continental arc volcanoes: evidence from Alicudi, Aeolian arc (southern Tyrrhenian Sea, Italy). *Journal of Petrology* **33**, 1295–1315.

Peccerillo, A., Kempton, P. D., Harmon, R. S., Wu, T. W., Santo, A. P., Boyce, A. J. & Tripodo, A. (1993). Petrological and geochemical characteristics of the Alicudi volcano, Aeolian islands, Italy: implications for magma genesis and evolution. *Acta Vulcanologica* **3**, 235–249.

Perez, W. A. & Dunn, T. (1996). Diffusivity of Sr, Nd and Pb in natural rhyolite melt at 1 GPa. *Geochimica et Cosmochimica Acta* **60**, 1387–1397.

Pichler, H. (1980). The island of Lipari. *Rendiconti Società Italiana di Mineralogia e Petrologia* **36**(1), 415–440.

Rottura, A., Del Moro, A., Pinarelli, L., Petrini, R., Peccerillo, A., Caggianelli, A., Bargossi, G. M. & Piccaretta, G. (1991). Relationships between intermediate and acidic rocks in orogenic granitoids suites: petrological, geochemical and isotopic (Sr, Nd, Pb) data from Capo Vaticano (southern Calabria, Italy). *Chemical Geology* **92**, 153–176.

Sawka, W. N. (1988). REE and trace element variations in accessory minerals and hornblende from the strongly zoned McMurry Meadows Pluton, California. *Transactions of the Royal Society of Edimburgh, Earth Sciences* **79**, 157–168.

Sawyer, E. W. (1991). Disequilibrium melting and the rate of melt–residuum separation during migmatization of mafic rocks from the Grenville Front, Quebec. *Journal of Petrology* **32**, 701–738.

Sawyer, E. W. (2001). Melt segregation in the continental crust: distribution and movement of melt in anatectic rocks. *Journal of Metamorphic Geology* **19**, 291–309.

Schenk, V. (1984). Petrology of felsic granulites, metapelites, metabasics, ultramafic and metacarbonates from Southern Calabria (Italy): prograde metamorphism, uplift and cooling of a former lower crust. *Journal of Petrology* **25**, 255–298.

Schiano, P. & Bourdon, R. (1999). On the preservation of mantle information in the ultramafic nodules: glass inclusions within minerals versus interstitial glasses. *Earth and Planetary Science Letters* **169**, 173–188.

Sisson, T. W. & Grove, T. L. (1993). Temperature and H_2O contents of low-MgO high-alumina basalts. *Contributions to Mineralogy and Petrology* **113**, 167–184.

Smith, V. G., Tiller, W. A. & Rutter, J. W. (1955). A mathematical analysis of solute redistribution during solidification. *Canadian Journal of Physics* **33**, 723–745.

Sobolev, A. V. & Danyushevsky, L. V. (1994). Petrology and geochemistry of boninites from the north termination of the Tonga trench: constraints on the generation conditions of primary high-Ca boninite magmas. *Journal of Petrology* **35**, 1183–1211.

Sobolev, A. V. & Slutskii, A. B. (1984). Composition and crystallisation conditions of the initial melt of the Siberian meimechites in relation to the general problem of ultrabasic magmas. *Soviet Geology and Geophysics* **25**, 93–104.

Sobolev, A. V., Hofman, H. C. & Nikogosian, I. K. (2000). Recycled oceanic crust observed in 'ghost' plagioclase within the source of Mauna Loa lavas. *Nature* **404**(6781), 986–990.

Stormer, J. C. & Nicholls, J. (1978). XLFRAC: a program for interactive testing of magmatic differentiation models. *Computers and Geosciences* **4**, 143–159.

Turner, S. & Foden, J. (2001). U, Th and Ra disequilibria, Sr, Nd and Pb isotope and trace element variations in Sunda arc lavas: predominance of a subducted sediment component. *Contributions to Mineralogy and Petrology* **142**, 43–57.

Van Dijk, J. P. & Scheepers, P. J. J. (1995). Neotectonic rotations in the Calabrian Arc: implications for a Pliocene–Recent geodynamic scenario for the central Mediterranean. *Earth-Science Reviews* **39**, 207–246.

Vroon, P. Z., van Bergen, M. J., White, W. M. & Varekamp, J. C. (1993). Sr, Nd and Pb isotope systematics of the Banda arc, Indonesia: combined subduction and assimilation of continental material. *Journal of Geophysical Research* **98**, 22349–22666.

Watt, G. R. & Harley, S. L. (1993). Accessory phase controls on the geochemistry of crustal melts and restites produced during water undersaturated partial melting. *Contributions to Mineralogy and Petrology* **101**, 220–231.

Watson, E. B. (1985). Henry's behaviour in simple systems and in magmas: criteria for discerning concentration-dependent partition coefficients in nature. *Geochimica et Cosmochimimica Acta* **49**, 917–923.

Watson, E. B. & Harrison, T. M. (1983). Zircon saturation revisited: temperature and composition effects in a variety of crustal magma types. *Earth and Planetary Science Letters* **64**, 295–304.

Wood, D. A., Joron, J. L., Treuil, M., Norry, M. & Tarney, J. (1979). Elemental and Sr isotope variations in basic lavas from Iceland and the surrounding ocean floor. *Contributions to Mineralogy and Petrology* **70**, 319–339.

Zanon, V., Frezzotti, M. L. & Peccerillo, A. (2003). Magmatic feeding system and crustal magma accumulation beneath Vulcano Island (Italy): evidence from CO_2 fluid inclusions in quartz xenoliths. *Journal of Geophysical Research* **108**(B6) 2298.